UNIVERSITY OF IOANNINA
PHYSICS DEPARTMENT
NUCLEAR PHYSICS LABORATORY

Study of the ^{162}Er(n,2n)^{161}Er reaction at near threshold energies

M.Sc. Thesis
Efstathia Georgali

Academic supervisor: Nikolas Patronis

Ioannina, February 2017

Μελέτη της αντίδρασης ^{162}Er(n,2n)^{161}Er κοντά στο ενεργειακό κατώφλι

ΜΕΤΑΠΤΥΧΙΑΚΗ ΔΙΠΛΩΜΑΤΙΚΗ ΕΡΓΑΣΙΑ

Ευσταθία Γεωργαλή

Ακαδημαϊκός επιβλέπων : Νικόλας Πατρώνης

Ιωάννινα, Φεβρουάριος 2017

Ευχαριστίες

Θα ήθελα να εκφράσω την ευγνωμοσύνη μου στον Επ. Καθ. Νικόλα Πατρώνη του Τμήματος Φυσικής, του Πανεπιστημίου Ιωαννίνων, που επέβλεψε αυτή την εργασία. Κατ' αρχάς του χρωστάω ένα μεγάλο ευχαριστώ για την εμπιστοσύνη που μου έδειξε και για την ευκαιρία που μου προσέφερε να δουλέψω πάνω σε αυτό το κομμάτι της Πυρηνικής Φυσικής, που λέγεται Πυρηνικές Αντιδράσεις. Ακόμη, θέλω να τον ευχαριστήσω για τον ενεργό ρόλο και τη προθυμία του να βοηθήσει σε όλες δυσκολίες της πειραματικής ανάλυσης, αλλά και για τις γνώσεις που με βοήθησε να αποκομίσω από αυτόν.

Ακόμη, θέλω να ευχαριστήσω την φίλη και συναδελφό μου Ζηνοβία Ελεμέ, επίσης μεταπτυχιακή φοιτήτρια του Τομέα Πυρηνικής Φυσικής, του Τμήματος Φυσικής, του Πανεπιστημίου Ιωαννίνων. Την ευχαριστώ για την βοήθεια της στη διεκπεραίωση αυτής της εργασίας, για τις εποικοδομητικές συζητήσεις που κάναμε μαζί πάνω σε ζητήματα της πειραματικής ανάλυσης αλλά και για τις όμορφες στιγμές που είχαμε δουλεύοντας μαζί.

Acknowledgements

I would like to express my gratitude to Assistant Prof. Nikolas Patronis, who supervised this thesis. First of all, I owe him a thank you for the confidence he showed me and the opportunity he gave me to work on this part of Nuclear Physics, called Nuclear Reactions. Moreover, I want to thank him for his active part and willingness to help in every experimental analysis difficulty, but also for the knowledge he helped me to derive from him.

Moreover, I want to thank my friend and colleague Zinovia Eleme, also being a postgraduate student at the Nuclear Physics Laboratory at the Physics Department of the University of Ioannina. I thank her for her assistance to the prosecution of this study, the constructive conversations we had on experimental analysis issues and the beautiful time we had working together.

Περίληψη

Η ενεργός διατομή της αντίδρασης ^{162}Er(n,2n)^{161}Er προσδιορίστηκε πειραματικά με την τεχνική της ενεργοποίησης για τρεις ενέργειες δέσμης νετρονίων κοντά στο ενεργειακό κατώφλι. Ο προσδιορισμός της ενεργούς διατομής έγινε σε σχέση με τις αντιδράσεις αναφοράς: ^{197}Au(n,2n)^{196}Au, ^{93}Nb(n,2n)^{92m}Nb και ^{27}Al(n,α)^{24}Na. Η ημί-μονό-ενεργειακή δέσμη νετρονίων παράχθηκε μέσω της αντίδρασης ^{2}H(d,n)^{3}He στον επιταχυντή Tandem Van der Graaf 5.5 MV του Ινστιτούτου Πυρηνικής και Σωματιδιακής Φυσικής του Ε.Κ.Ε.Φ.Ε "Δημόκριτος",χρησιμοποιώντας αέριο στόχο δευτερίου. Μετά το τέλος κάθε ακτινοβόλησης πραγματοποιήθηκε η μέτρηση της ενεργότητας των δειγμάτων. Λόγω της ελάχιστης περιεκτικότητας του στόχου Ερβίου σε ^{162}Er για τις μετρήσεις της ενεργότητας χρησιμοποιήθηκαν δύο ανιχνευτές γερμανίου HPGe , όπου ο καθένας είχε σχετική απόδοση 100%, ενώ για τους στόχους αναφοράς χρησιμοποιήθηκε ένας ανιχνευτής γερμανίου HPGe με σχετική απόδοση 16%. Από την παρούσα εργασία προέκυψαν τα πρώτα πειραματικά δεδομένα για τις εξής ενέργειες δέσμης νετρονίων : 10.7 MeV, 11.0 MeV και 11.3 MeV.

Abstract

The ^{162}Er(n,2n)^{161}Er reaction cross section was experimentally determined by means of the Activation Technique relative to the ^{197}Au(n,2n)^{196}Au, ^{93}Nb(n,2n)^{92m}Nb and ^{27}Al(n,α)^{24}Na reference reactions at near threshold energies. The quasi-mono-energetic neutron bean was produced via the ^{2}H(d,n)^{3}He reaction at the 5.5 MV Tandem Van der Graaf accelerator of the Institute of Nuclear and Particle Physics at N.C.S.R. "Demokritos", using gas deuterium target. After each irradiation, the targets' induced activity was measured. Due to the minimal abundance of ^{162}Er in the natural erbium target for the activity measurements two 100% relative efficiency HPGe detectors were used in close geometry, whereas for the activity measurements of the reference foils one 16% HPGe detector was used. From the present work the ^{162}Er(n,2n)^{161}Er reaction cross section was determined for the first time at the following neutron beam energies : 10.7 MeV, 11.0 MeV and 11.3 MeV.

Contents

1. Introduction

1.1 Motivation

The experimental and theoretical study of nuclear reactions cross sections is one of the primary goals of the nuclear physics research. Investigation on nuclear reaction mechanisms contributes not only to a better understanding of the nuclear reactions models and the role of nuclear structure, but also to the development and improvement of many applications.

Within the present work the experimental study of the ^{162}Er(n,2n)^{161}Er reaction is presented. Neutron induced nuclear reactions with rare earth elements are in general of special interest for basic research purposes as well as for the development of nuclear physics applications. ^{162}Er is the lightest Erbium isotope with minimal abundance (0.139 %). Although, ^{162}Er is a stable isotope still is a proton rich nucleus quite far from the mainstream of the valley of stability. Accordingly, its determination of cross section will help for a better understanding of Compound Nucleus reaction theory and its decay mechanisms. Moreover, the exact knowledge of the experimental values of the cross section will help for the determination of the semi-empirical parameters of the Hauser-Feschbach theory equations which are necessary for the theoretical estimations. This procedure will improve the theoretical models and will demonstrate the most suitable ones for the forecast of similar reactions cross sections for nuclei in the this region of the chart of nuclides.

Moreover, nuclear reactions of Erbium isotopes are important due to their high neutron capture cross sections. This fact makes Erbium one of the best materials to be used as neutron absorber in fast neutron reactors [1]. The fast neutron reactors differ with the conventional ones in the fact that they do not use any moderator (commonly water) to slow down the neutrons produced from fission so as to sustain the nuclear chain reaction. In contrast they operate at fast neutron energies. Recently, fast neutron reactors seem to gain their old fame and be a promising technology for power production because of their three major advantages [2]:

- they can solve the problem of "fuel shortage" as they permit fuel to be bred from almost all the actinides. On average, more neutrons per fission are produced from fissions caused by fast neutrons than from them caused by thermal neutrons. This results in a larger surplus of neutrons beyond those required to sustain the chain reaction. These neutrons can be used to produce extra fuel (fast breeder reactors - FBR).

- Fast neutron reactors are also effective to burn the long-lived minor actinides of radioactive waste. Actinides have a higher fission cross section at fast energies than at thermal energies. After fission actinides become a pair of "fission products", which have decreased half-life time from some million years to a few centuries.

- Generally, neutron capture rates are lower as the energy of neutron is increased. Therefore, the transuranic radio-toxicity of the produced nuclear wastes is significantly reduced.

1.2 Previous experimental data of the ^{162}Er(n,2n)^{161}Er reaction cross section

Concerning the EXFOR data base the ^{162}Er(n,2n)^{161}Er reaction has been unexplored for a wide energy range, since the only existing experimental data are limited in the energy range between 13.5-15 MeV ([3]-[11]). This inhibits the accurate benchmarking of the theoretical calculations. Things are made even more difficult because of the discrepancies between the experimental data which approach even the 30 %. So, it can be said that the ^{162}Er(n,2n)^{161}Er reaction is still in a primitive stage of study.

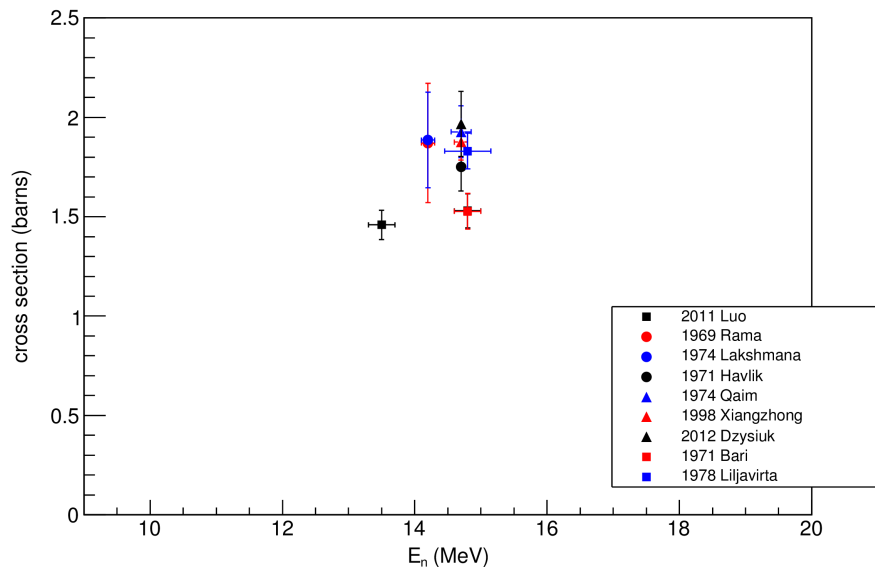Figure 1.1: experimental data of previous studies of the ^{162}Er(n,2n)^{161}Er reaction concerning the EXFOR data base.

Within the present work the measurement of the ^{162}Er(n,2n)^{161}Er reaction cross section at energies just above the threshold (Q_{th}=9.262 MeV) is presented. According to our knowledge the experimental data of the present work are the first data in this energy region.

1.3 Nuclear Reaction Mechanisms

The nuclear reactions are classified into categories according to the mechanisms of interaction between the projectile and the target-nucleus [12] :

- Direct reactions
- Compound Nucleus reactions

The Direct reactions are peripheral reactions, due to the fact that the projectile, primarily, interacts with the nucleons in the surface of the target-nucleus. In this case the interaction takes place quickly in a time scale of 10^{-22} s. This time is not enough for the projectile to lose its entire energy, but only a portion of it is shared among the target's peripheral nucleons. Due to their small duration and the partial decrease in the projectile's energy, the products of these reactions are strongly depend on the interacting nuclei.

Direct Reactions are classified into four subcategories:

1. Elastic scattering: In this case the nucleons are not exchanged between the projectile and the target nuclei. Only the kinetic energy of the projectile and its emission angle are changed.
2. Inelastic scattering: In this case also there is no exchange of nucleons . However, part of the kinetic energy is transferred to the bound nucleons exciting the colliding nuclei..
3. Stripping reactions: some nucleons are transferred from the projectile to the target.
4. Pick up reactions: it is the opposite procedure. In this case the nucleons are transferred from the target to the projectile.

On the other hand, in Compound Nucleus reactions, the projectile interacts with the whole nucleus. The projectile's energy is shared among all the nucleons of the target via nucleons-nucleons reactions, until thermodynamical equilibrium is reached. This means that the projectile is absorbed by the target-nucleus until a compound, highly excited nucleus with lifetime equal to $t \simeq 10^{-16}$ is formed. In other words the projectile loses its " identity " and the compound nucleus may be said that have lost memory of the particular input channel of formation. The compound nucleus is in an excited state and de-excites (“evaporates”) in a way that doesn't depend on the input channel. This principle is called Bohr hypothesis. Bohr' hypothesis mathematical formalism is:

$$\sigma_{ab} = \sigma_{aC} G_b \quad \text{(eq. 1.1)}$$

where, σ_{aC} describes the cross section of the formation of the compound nucleus and G_b its decay probability. The term G_b is expressed as the quotient of the partial decay width:

$$G_b = \frac{\Gamma_b}{\Gamma} \quad \text{(eq 1.2)}$$

The intermediate mechanism between the two extremes (compound nucleus and direct reactions) are the pre-equilibrium reactions . In these reactions during the nucleon-nucleon interactions, some nucleons or light nuclei acquire enough energy to escape from the complex system target-projectile before the equilibrium is reached. Due to this, there is not total independence between the formation and de-excitation of the target-projectile complex system, but the Compound nucleus “conserves some memory”.

Compound Nucleus reactions vs Direct reactions

Although there are no strict boundaries between the direct and the compound reaction mechanisms, the primary parameter that finally determines the mechanism of the reaction is the center-of-mass kinetic energy. Compound Nucleus reactions are favored in lower energies, whereas Direct reactions is the dominant reaction mechanism at higher energies. More specifically, the lower the energy is the larger the wave-length λ of the particle will be (λ=h/p). So, it is easier for the projectile to interact with the whole target and a Compound nucleus to be formed. Respectively, for higher energies the wave-length of the projectile is smaller limiting the interaction with only some peripheral nucleons of the target. It is obvious that the pre-equilibrium reaction mechanism regime are the intermediate energies. This is the reaction that bridges the two extreme cases of nucleus-nucleus interaction.

1.4 The ^{162}Er+n interaction

The ^{162}Er+n interaction is dominated by the compound nucleus reaction mechanism, which leads the formation of the ^{163}Er* nucleus.

Following the compound nucleus formation in the table given below the different reaction channels are presented:

output channels	Q-value (MeV)	
^{162}Er+n	0	elastic scattering
^{161}Er+2n	-9.20	endothermic
^{160}Er+3n	-16.41	endothermic
^{159}Er+4n	-25.99	endothermic
^{162}Ho+p	0.49	exothermic
^{161}Ho+n+p	-6.43	endothermic
^{159}Dy+α	8.48	exothermic
^{158}Dy+n+α	1.65	exothermic
^{161}Ho+d	-4.2	endothermic
^{160}Ho+t	-6.83	endothermic

Table 1.1: possible output channels of the ^{162}Er +n compound nucleus reaction

where Q-value is the energy absorbed (endothermic reaction) or released (exothermic reaction) during the reaction

$$Q(MeV) = \Delta(reactive\,nuclei) - \Delta(product\,nuclei) \quad \text{(eq. 1.3)}$$

whereas Δ is the total mass excess of the initial and product nuclei.

1.5 Energy diagram of the ^{162}Er+n interaction

The ^{163}Er* nucleus is a compound nucleus , which is produced from the ^{162}Er+n interaction in a high excited state with excitation energy E_x:

$$E_x = S_n + E_{n,CMS} \quad \text{(eq 1.4)}$$

where S_a is the neutron binding energy in the ^{163}Er* nucleus and $E_{n,CMS}$ is neutron beam energy (bombarding energy) at the Center of Mass (CM) System

The neutron binding energy is given from the equation:

$$S_n = \Delta(^{162}Er) + \Delta(n) - \Delta(^{163}Er) \Rightarrow S_n = (-66.33\,MeV) + (8.07\,MeV) - (-65.17\,MeV)\,V \Rightarrow S_n = 6.90\,MeV$$
(eq 1.5)

The CM neutron energy depends on the laboratory neutron beam energy via the equation:

$$E_{n,CMS} = \frac{A_{RN}}{A_{CN}} E_{Lab} \quad \text{(eq. 1.6)}$$

where A_{RN} is the mass number of the target nucleus (A_{RN}=162) and A_{CN} is the mass number of the compound nucleus (A_{CN}=163).

Consequently, for the three irradiations:

En (MeV) at lab	$E_{n,CMS}$ (MeV)
10.7	10.6
11.0	10.9
11.3	11.2

Table 1.2: neutron beam energies at CMS for each irradiation

and the excitation energies for each irradiation are:

En (MeV)	excitation energy (MeV)
10.7	17.5
11.0	17.8
11.3	18.1

Table 1.3: excitation energies of ^{163}Er* compound nucleus for each irradiation energy

According to the information with respect to the excitation energy of the compound nucleus as presented previously and the required energy for each reaction channel as presented below, the energy

diagram of the n+^{162}Er reaction can be formed (Figure 1.2).

output channels	energy levels (MeV)
^{162}Er+n	6.90
^{161}Er+2n	16.10
^{160}Er+3n	23.31
^{159}Er+4n	32.89
^{162}Ho+p	6.41
^{161}Ho+n+p	13.33
^{159}Dy+α	-1.58
^{158}Dy+n+α	5.25
^{161}Ho+d	11.10
^{160}Ho+t	13.73

Table 1.4: the possible reaction channels of the interaction between the ^{162}Er and the neutron in accordance with the ^{163}Er* level.

Where for the energy level determination it was applied the equation:

$$Q(MeV) = \Delta(^{163}Er) - \Delta(reactive\ nuclei)\quad\text{(eq. 1.7)}$$

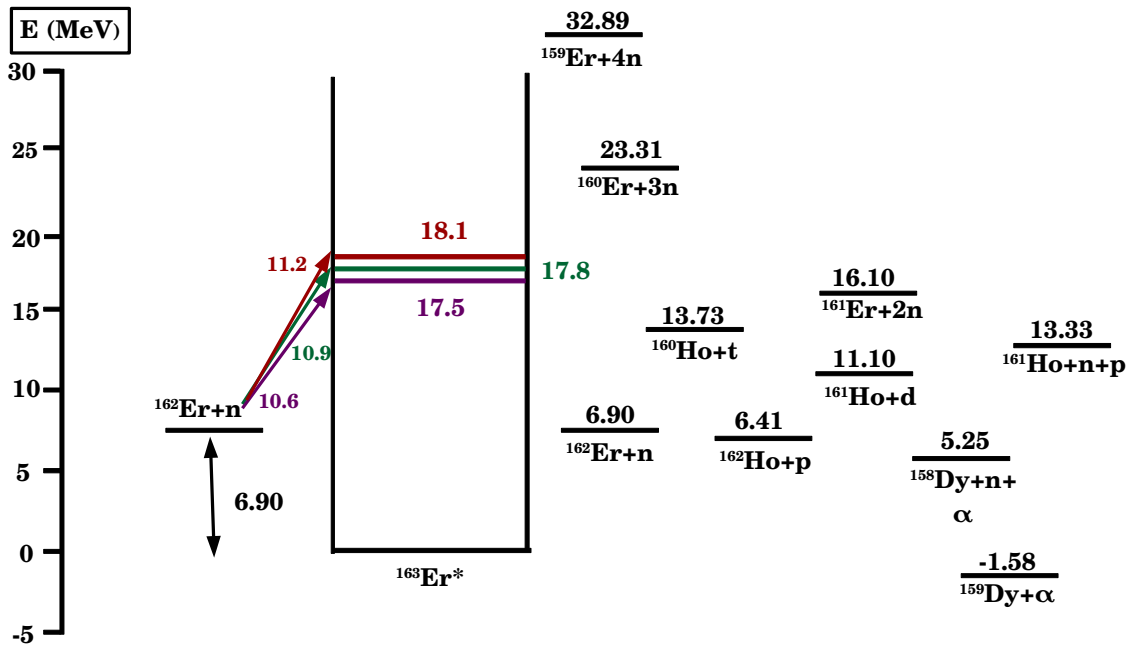Here the term Q corresponds to the excitation of the compound nucleus ^{163}Er* for zero beam energy.

Figure 1.2: enery diagram of the ^{162}Er+n interaction

2. Experimental Set-up and Method

2.1 Activation Technique

The Activation Technique is an established technique for the determination of the reaction cross section. The high sensitivity and selectivity of the method has been proven [13]. This method can be implemented in those physics cases where the product nucleus of the reaction under study is an unstable nucleus with suitable decay parameters (intensity, energy, decay mode, half-life, etc) [14]. More specifically, the activation technique consists of two stages: Firstly, the sample-target is irradiated by mono-energetic particle-beam. The target material as well as the particle beam depends on the reaction under study. During the irradiation the unstable product nuclei are formed. After the irradiation the induced activity with respect to the population of the product nucleus of the reaction under study is measured. Accordingly, the cross section can be obtained using the following equation.:

$$\sigma = \frac{A \, CF_{SA} \, CF_{DT}}{N_T \, \Phi \, \varepsilon \, I_\gamma (1 - e^{-\lambda t_m}) e^{-\lambda t_w} f_b} \quad \text{(eq 2.1)}$$

where A , the induced daughter's nucleus Activity
Φ, the irradiation flux
N_T, the initial number of stable nuclei in the irradiation sample
I , the emitted ray's intensity
ε, detector's efficiency for the emitted radiation
λ, the decay constant of the daughter nucleus
t_m, the measuring time of the induced activity
t_w, the waiting time between the end of the irradiation and the start of measurement
CF_{SA}, the sample's self-attenuation correction factor
CF_{DT}, the detector's dead time correction factor
f_b, the correction factor for the daughter nuclei decay during irradiation

For constant flux: $fb = \frac{(1 - e^{-\lambda t_{ir}})}{\lambda t_{ir}}$ (eq. 2.2) , whereas for non-constant flux: $fb = \frac{\int_0^{t_{ir}} f(t) e^{\lambda t} \, dt}{\int_0^{t_{ir}} f(t)} e^{-\lambda t_{ir}}$

(eq. 2.3)

After the irradiation the population of the reaction product has to be determined. Therefore, for the daughter nucleus activity off-line measurements are conducted. This sets a limit to the application of the Activation Technique. More specifically, the daughter nucleus half-life time has to be long enough. This ensures that the nuclei will not decay just after the irradiation stops, before the activity measurement takes place. However, the half-life time cannot be very long as well. In such a case, a long irradiation and measuring time are necessary for achieving a reasonable decay rate and to obtain a sufficiently adequate statistics.

The off-line measurements , despite the afore mentioned limitations with respect the decay characteristics, have an important advantage. Given that the off-line measurements is free from any

beam-related background results in significant improved signal-to-background ratio thus increasing the selectivity and sensitivity of the measurement.

Another consideration when Activation Technique is applied, is the absence of interference reactions. Before applying the Activation Technique it has to be ensured that there are no reactions producing the same isotope as the one being populated by the reaction of interest.

The equation (2.1) combines three magnitudes: the cross section σ of the reaction under study, the irradiation flux Φ and the number of target nuclei N_T. This means that if two of the three are known each time, the third can be easily calculated. Usually, the final goal of an experiment is the reaction cross section determination.

The number of the target nuclei in the sample N_T is equal to:

$$N_T = a\,v\,\frac{m\,N_A}{MW} \quad (2.4)$$

where, α the abundance of the mother nucleus in the natural composition
ν, the number of atoms of the nucleus of interest in the molecular used as target material
m , the sample's mass
N_A, the Avogadro number
MW, the molecular weight of nuclei contained into the sample (the sample may contain different elements)

It has to be mentioned that it is important that the sample radius is smaller than the beam radius as to be fully irradiated from the neutron beam. Otherwise in the calculation the sample mass corresponding to the beam profile has to be taken into account.

Considering the flux Φ, in most of the neutron physics experiments it cannot be measured directly. In such cases, flux is calculated using reference foils . These foils are placed front and back of the main sample ("sandwich technique"), so as to be irradiated by the beam as well. The induced reactions must lead to the formation of daughter nuclei with adequate half-life times and have a well known cross section. If these requirements and the rest mentioned above are fulfilled, the flux can be calculated as the inverse solution of the equation (2.1) mentioned at the begin of this chapter:

$$\Phi = \frac{A\,CF_{SA}\,CF_{DT}}{N_T\,\sigma\,\varepsilon\,I_\gamma\left(1 - e^{-\lambda t_m}\right)e^{-\lambda t_w}f_b} \quad (2.5)$$

2.2 Erbium target and reference foils

The ^{163}Er* compound nucleus produced after the interaction between the ^{162}Er and the neutron is decayed by the emissions of two neutrons. The ^{161}Er nucleus formated in the sample is unstable with half-life time $T_{1/2}$=3.21 h and it is decayed by 100% electron capture towards to ^{161}Ho. The ^{161}Ho decays to the ground state through γ-ray emissions. Because of the large number of γ-rays the ^{161}Er decay scheme is complicated enough. Among of the γ-rays emitted the stronger one and the one used within the present work is at E_γ=826.6 keV with intensity I=64% (4) [15].

The neutron flux was estimated by the following reference reactions:

- ^{27}Al(n,a)^{24}Na,   Q=-3.132 MeV
- ^{197}Au(n,2n)^{196}Au,   Q=-8.072 MeV
- ^{93}Nb(n,2n)^{92m}Nb,   Q=-8.830 MeV

The decays of the unstable nuclei produced are described by the following decay-schemes:

- ^{24}Na daughter nucleus

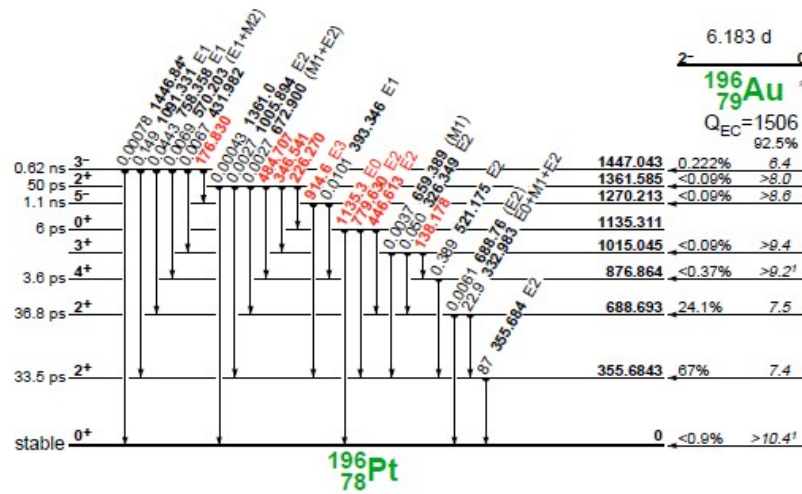Figure 2.1: decay scheme of ^{24}Na unstable nucleus

- ¹⁹⁶Au daughter nucleus

Figure 2.2: decay scheme of ¹⁹⁶Au unstable nucleus

- ⁹²ᵐNb daughter nucleus
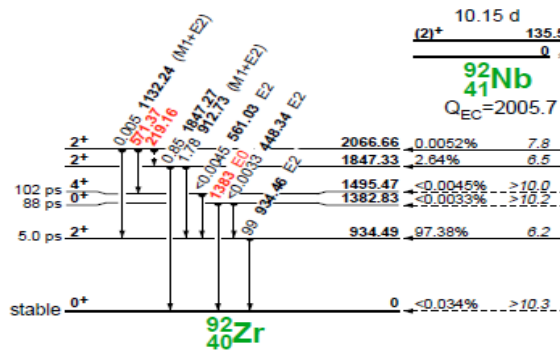
Figure 2.3: decay scheme of the ⁹²ᵐNb unstable nucleus

The γ-rays by which the reference foils activity was determined are mentioned in the table (2.1) ([16]-[18]):

reference foils	daughter nuclei	$T_{1/2}$	E_γ (keV)	I (%)	σ_I(%)
²⁷Al	²⁴Na	14.997 h	1368.626	99.9936	0.0015
¹⁹⁷Au	¹⁹⁶Au	6.1669 d	333.03	22.881	0.946
⁹³Nb	⁹²ᵐNb	10.15 d	934.44	99.15	-

Table 2.1: γ-rays emitted during the reference foils' daughter nuclei decay

2.3 Neutron beam

The neutron beams are always secondary beams produced by a variety of nuclear reactions depending on the primary beam characteristics, the neutron beam energy and the specific experimental conditions.

Within the present work the adopted reaction for the production of the quasi-mono-energetic neutron beams was:

$$_1^2H + _1^2H \rightarrow n + _2^3H$$
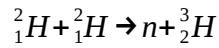
widely known as the D-D reaction. D-D is an exothermic reaction with Q-value=3.26 MeV

The deuterium beams were provided by the 5.5 MV Tandem Van der Graaf accelerator of the Institute of Nuclear and Particle Physics at N.C.S.R "Demokritos". The deuterium beam was directed and focused to a deuterium gas target. During the irradiations the gas target pressure was 1250 mbar. The gas pressure in the gas-shell was remotely controlled and was kept constant by means of a micro-metric vane.

Three irradiations were conducted at neutron energies of 10.7 MeV, 11.0 MeV and 11.3 MeV. The correspondence of the neutron beam energy with the deuterium beam energy is given on the Table 2.2.

E_d (MeV)	E_n (MeV)
7.86	10.7
8.17	11.0
8.47	11.3

Table 2.2: the deuterium bombarding energies and the respective neutron energies produced

A simulation of the energy distribution of the neutrons produced for each deuterium irradiation was produced via the NeuSDesc code [19], which confirmed the values of the neutron beams energies:

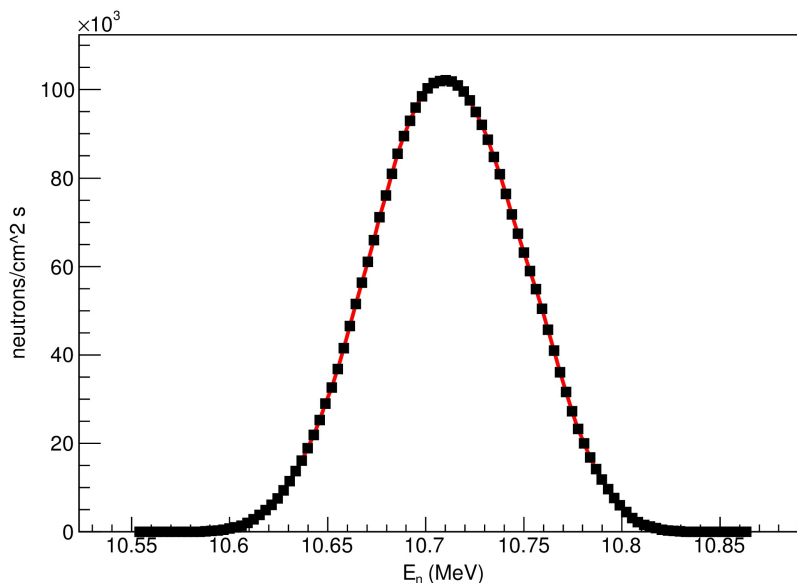- for E_d=7.86 MeV

Figure 2.4: neutron energy distribution for bombarding deuterium energy E_d=7.86 MeV
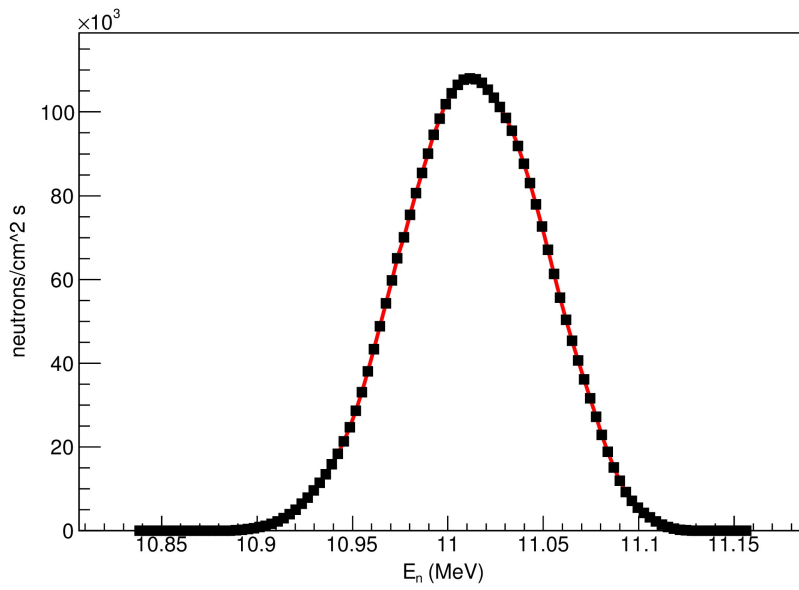
- for E_d=8.17 MeV,

Figure 2.5: neutron energy distribution for bombarding deuterium energy E_d=8.17 MeV
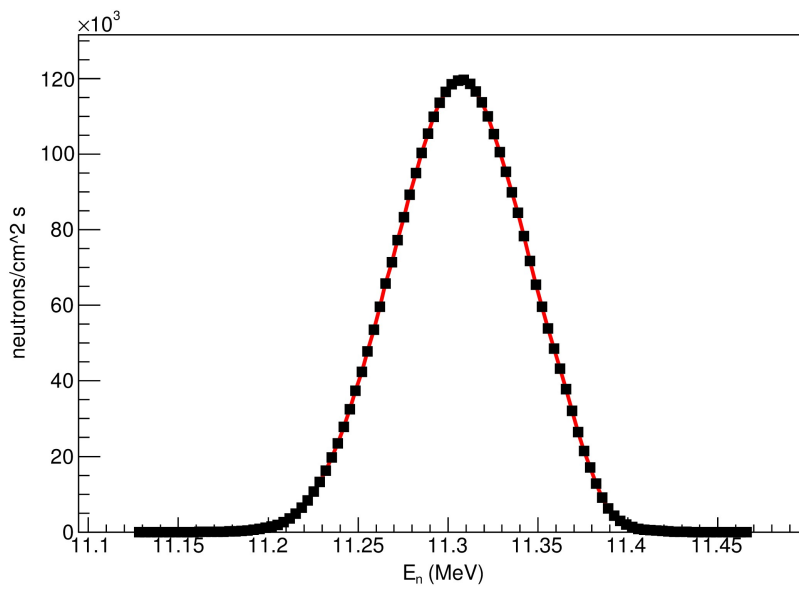
- for E_d=8.47 MeV

Figure 2.6: neutron energy distribution for bombarding deuterium energy E_d=8.47 MeV

2.4 Neutron beam fluctuations and BF$_3$ Detector

In order to take into account in an accurate way the decay of the product nuclei during the irradiation the neuron beam intensity-fluctuations have to be recorded by means of a Multi-Channel-Scaller. For this reason a BF$_3$ detector was used as neutron counter.

BF$_3$ detector's function:

The BF$_3$ detector is as a proportional counter, which is filled with BF$_3$ gas, usually enriched to more than 90 percent in ^{10}B. The neutron detection is based on the following reaction :

$$^{10}B + n \rightarrow ^4He + ^7Li$$
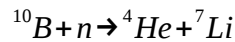
The above reaction is an exothermic reaction and concerning whether the ^{7}Li is formed in the ground or in an excited state it has different Q-values:

- ^{7}Li at ground state: Q-value=2.792 MeV
- ^{7}Li at excited state: Q-value=2.31 MeV   (0.480 MeV is converted into ^{7}Li excitation energy ➜ less energy is emitted)

In the 94 % of the reactions the ^{7}Li is left in an excited state, whereas the rest 6 % of them leave ^{7}Li in the ground state.

The alpha and ^{7}Li particles produced are emitted at opposite directions (linear momentum conservation).
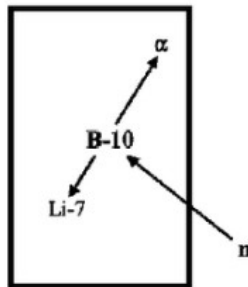
Figure 2.7: the alpha and ^{7}Li particles produced at the BF$_3$ detectors travel off at opposite directions

During their transportation inside the gas, the alpha and ^{7}Li particles ionize the gas and create primary ion pairs. The electrons from the primary ion pairs create further "secondary" ion pairs as they get close to the anode (avalanche electrons).

The electrons are approaching the anode and the positive charged ions are moving towards the cathode. In this way, pulses are created. Their size depends on whether the ^{7}Li is formed at the ground or at the excited state. In the first case, the alpha and ^{7}Li particle have more kinetic energy and ,consequently, a higher pulse results. Respectively, the pulse has a smaller height when ^{7}Li is excited.

The $^{10}B(n,\alpha)^7Li$ reaction cross section has an energy dependence equal to $1/\sqrt{E_n}$. For this reason, BF_3 counters, almost exclusively, respond to thermal neutrons,whereas the cross section for the absorption of fast neutrons by ^{10}B is much smaller. Therefore, as to increase the intrinsic detection efficiency the incident neutrons are moderated. For this reason the BF_3 gas counter is placed inside a paraffin moderator in barrel configuration. For the same reason any information for the initial kinetic energy of the neutrons finally lost thought the moderation process.

Neutron flux fluctuations recorded by the BF_3 counter

During the irradiations the neutron flux was recorded by means of a Multi-Channel- Scaler. Every 60 sec the total number of pulses were recorded.

- Neutron Irradiation Energy:
  10.7 MeV
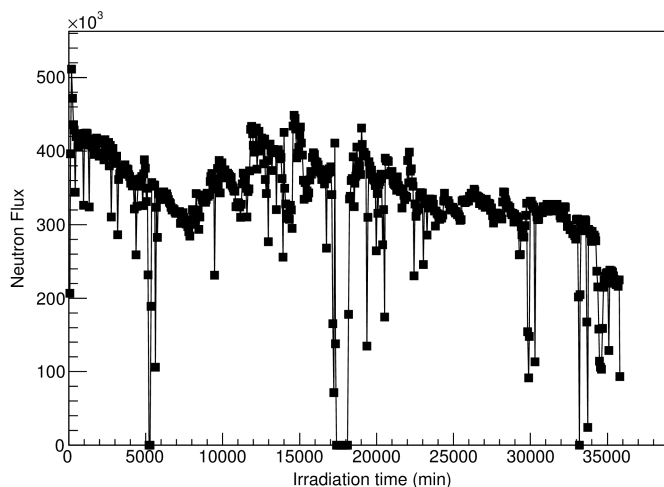
Figure 2.8: neutron fluctuations as recorded from the BF_3 counter for E_n=10.7 MeV

- Neutron Irradiation Energy
  11.0 MeV
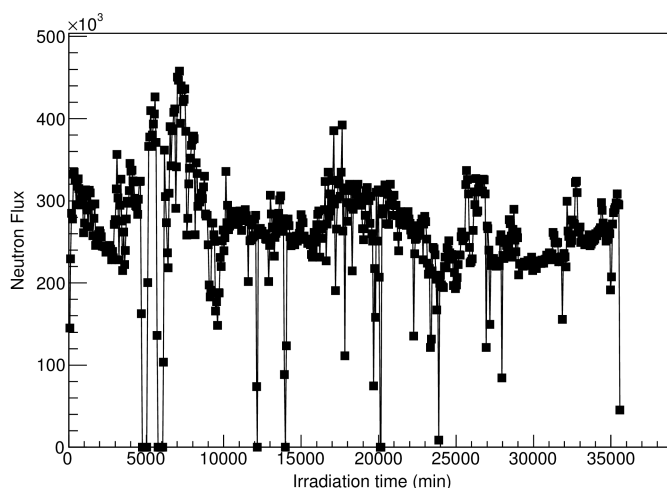
Figure 2.9: neutron fluctuations as recorded from the BF_3 counter for E_n=11.0 MeV

27

- **Neutron Irradiation Energy: 11.3 MeV**
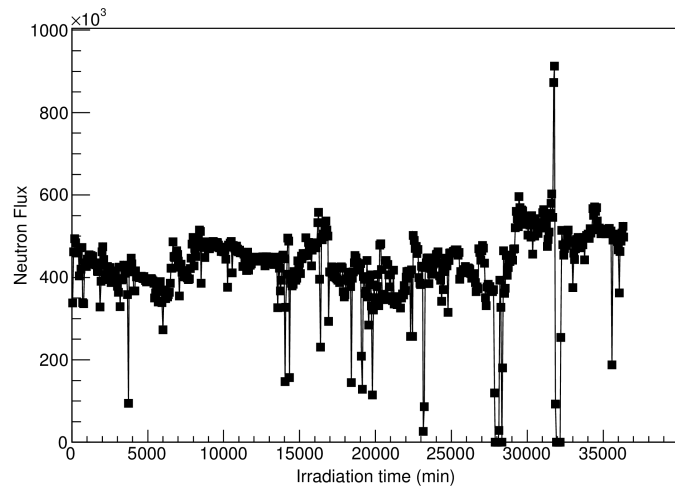
Figure 2.10: *neutron fluctuations as recorded from the BF_3 counter for $E_n=11.3$ MeV*

2.5 Irradiation Set-up

For the estimation of flux, reference foils of ^{27}Al, ^{197}Au and ^{93}Nb were used. They were placed front and back of the erbium pellet ("sandwich technique") at a distance of 5 cm from the D_2 gas target :
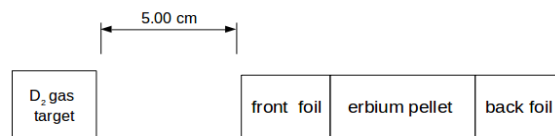
Figure 2.11: schematic representation of the reference foils and the erbium pellet place
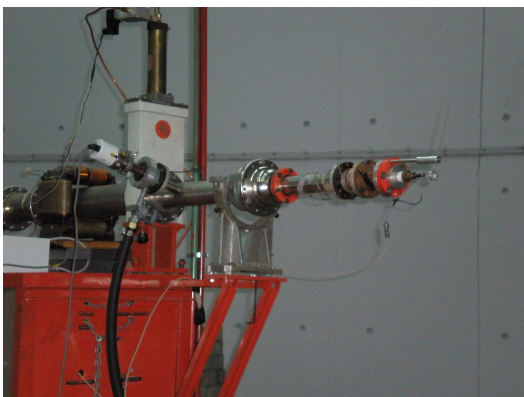
Figure 2.12: irradiation set-up

Figure 2.13: irradiation set-up

28

Each irradiation last about 10 h (~3$T_{1/2}$, 3 times the half-life time of ^{161}Er).

	E$_n$ (MeV)	Irradiation time (s)
first irradiation	10.7	35820
second irradiation	11.0	35580
third irradiation	11.3	36360

Table 2.3: irradiation times

In the irradiations two erbium targets were used:

	mass (mgr)	diameter (mm)	thickness (mm)
erbium target A	994.43	12.95	2.00
erbium target B	1059.65	12.95	1.99

Table 2.4: mass and geometrical characteristics of the erbium targets

2.6 γ-ray Detectors

After the irradiations, the induced activity of the erbium sample and the reference foils was measured using two100% relative efficiency HPGe and one 16% relative efficiency HPGe detectors.

Because of the minimal abundance of ^{162}Er in natural sample composition (0.139%) the maximum possible efficiency was necessary. For this reason, the ^{161}Er decay detection was carried out by the two HPGe detectors with 100% relative efficiency. They were placed in close geometry in a distance of some centimeters, whereas the erbium pellet was at the middle of this distance. In this way a solid angle ~4π was covered.

Figure 2.14: the 2x100% HPGe detectors used for the erbium pellet activity measurement

By measuring the γ-ray activity at close geometry the detection solid angle is increased and therefore the detection efficiency is also enhanced. On the other hand the issue of summing effects arises when a close detection geometry is adopted. For this reason the calibration of the detector was done by using a ^{54}Mn point source where a single γ-ray line at 835 keV- very close to the 827 keV decay line of ^{161}Er is emitted (see also next paragraph). Furthermore, despite the complexity of the ^{161}Er decay scheme the 827 keV line is emitted with multiplicity 1-(within ~1% approximation).

The reference foils' activity measurements were conducted by the 16% HPGe detector. The distance from the detector's window was at 7 cm. In this way it was ensured that the measurement was free from coincidence-summing effects. Because of the small half-life time of ^{24}Na (T$_{1/2}$=14.997 h), it was necessary the aluminum foils to be placed first at the detector and afterwards the rest.

Figure 2.15: the 16% HPGe detector used for the measurement of the foils activity

The three detectors were adjusted to operate simultaneously. Every hour the recorded spectra were saved and erased. In this way possible data loss was avoided and secondly the decay rate of the measured activity could be followed.

2.7 Detectors calibration

[161]Er decays through EC (100%) by feeding several excited states of the daughter nucleus [161]Ho resulting in a quite complicated decay scheme:
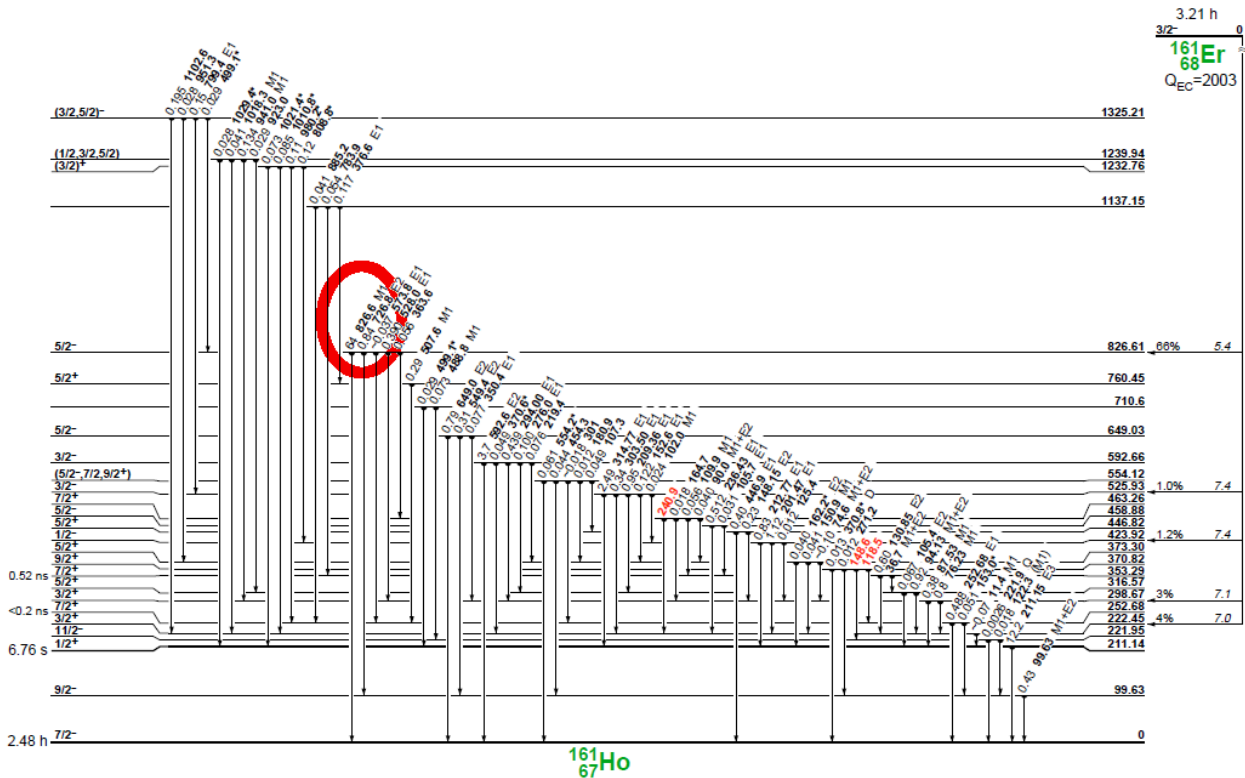
Figure 2.16: Decay Scheme of [161]Er

The [161]Ho nucleus decays to its ground state through the emission of several γ-rays, but the strongest one is 826.6 keV. For the calibration of the 2x100% HPGe detectors at this energy, a point [54]Mn source was placed between the 2x100% HPGe detectors at the same distance as the erbium pellet.

The [54]Mn is one of the unstable isotopes of Mn nuclei with half-life time $T_{1/2} = 312.20$ days. During its decay, it emits γ-rays of 834.8 keV energy with an intensity equal to 99.9760 % (10) [20]. The point source of [54]Mn was adopted for the calibration of the two 100 % HPGe detectors for two reasons: Firstly, the energy of the emitted photon is very close to the region of interest for the [161]Er decay (827 keV) and secondly is a mono-energetic γ-ray source. The fact that the γ-ray multiplicity is equal to one, as can be seen in Fig. 1.16, is important because corrections for coincidence summing effects are not needed.
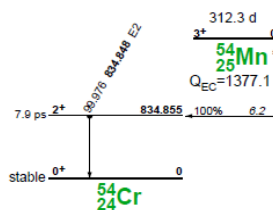
Figure 2.17: [54]Mn decay scheme

31

The 16% HPGe detector was calibrated in an extended energy range as to cover the detection needs for the used reference foils. For this purpose, a point source of ^{152}Eu was placed at distances of 7 cm and 13 cm from the detector's window. ^{152}Eu is one of the unstable isotopes of Eu with half-life time $T_{1/2}$= 13.517 years. It appears a quite complicated decay scheme, as is decayed by the emission of many strong γ-rays from some hundreds keV up to ~1400 keV [21].

3. Data Analysis

3.1 Calibration curves of 16% HPGe Detector

For the calibration curves of the16% HPGe detector a point source of ^{152}Eu was placed at 7 cm and at 13 cm distance from the detector's window. This source emits photons at different energies. The characteristics photon energies, the intensities and the corresponding uncertainties of ^{152}Eu are summarized in the Table 3.1 :

Eγ (keV)	I (%)	σ$_I$ (%)
244.6974	7.55	0.04
344.2785	26.59	0.21
443.9606	2.827	0.015
778.9045	12.93	0.09
964.057	14.51	0.07
1112.076	13.67	0.09
1408.013	20.87	0.10

Table 3.1: ^{152}Eu decay energies and the respective
intensities

A characteristic spectrum of ^{152}Eu decay is:
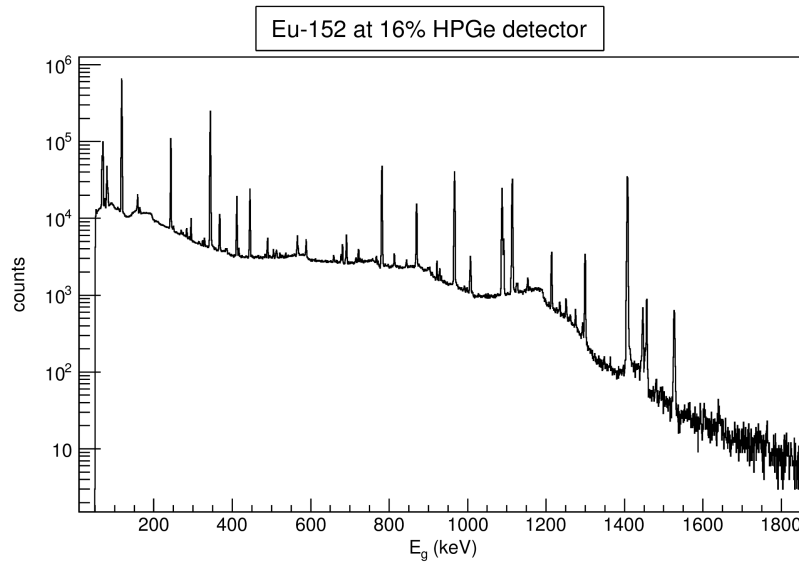
Figure 3.1: ^{152}Eu decay spectrum of 16% HPGe detector at 7 cm

A detector's efficiency is equal to the ratio of the counts detected to the total source's emissions at the detector's Data Acquisition Time (DAQ-time):

$$\varepsilon = \frac{counts}{emissions} \quad \text{(eq. 3.1)}$$

The photons emitted by the point source during DAQ-time are calculated via the equation:

$$emissions = A\, I\, DAQ-time \quad (3.2)$$

where A is the source's activity

The ^{152}Eu point source had known activity: $A_0 = (217 \pm 3)$ kBq at 01/01/2011. So the date of the experiment conduction at 12/02/2014 had activity equal to A=(185 ± 3) kBq , concerning the decay law:

$$A = A_o\, e^{-\lambda t} \quad (3.3)$$

where the decay constant $\lambda = (0.05128 \pm 0.00005)$ 1/years

t= 1138 days

In the following table the total counts', emissions' and efficiencies' results are presented with the respective errors :

- for 7 cm source-detector's window distance. The DAQ-time was considered equal to detector's live-time=2250.797 s (the part of the DAQ-time for which the detector's electronics were active). The DAQ dead-time correction factor was equal to 1.

Eγ (keV)	counts	σ_{counts}	emissions	$\sigma_{emissions}$	efficiency	$\sigma_{efficiency}$
244.6974	270128	697	31427363	465320	0.00860	0.00013
344.2785	676152	912	110682595	1742081	0.00611	0.00010
443.9606	58603	365	11767570	172819	0.00498	0.00008
778.9045	140796	451	53821961	815249	0.00262	0.00004
964.057	127984	418	60398814	884442	0.00212	0.00003
1112.076	106691	386	56902259	854299	0.00187	0.00003
1408.013	129429	367	86872725	1258161	0.00149	0.00002

Table 3.2: 16% HPGe detector efficiencies for ^{152}Eu decay energies at 7 cm
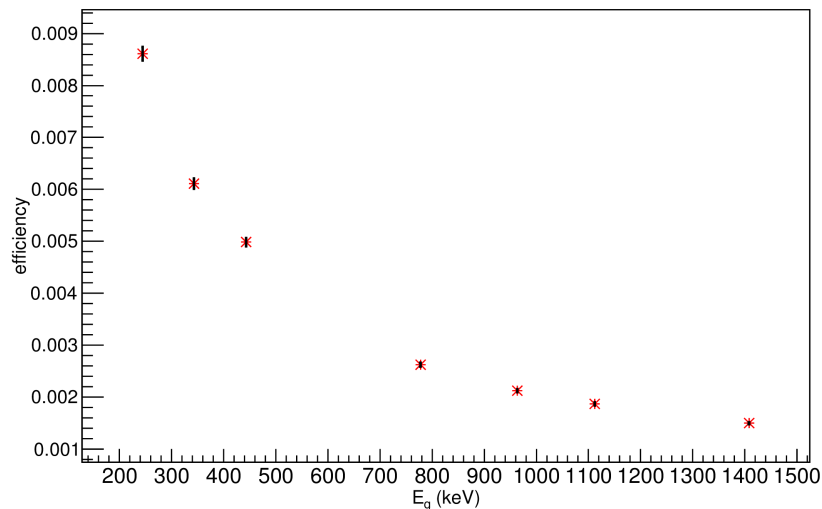
Figure 3.2: calibration curve of 16% HPGe detector at 7 cm

- for 13 cm source-detector's window distance and detector's live-time=4429.081 s

E_γ (keV)	counts	σ_{counts}	emissions	$\sigma_{emissions}$	efficiency	$\sigma_{efficiency}$
244.6974	211070	603	61842244	915649	0.00341	0.00005
344.2785	520819	797	217799374	3428038	0.00239	0.00004
443.9606	46510	315	23156030	340070	0.00201	0.00003
778.9045	111061	393	105909963	1604233	0.00105	0.00002
964.057	102680	366	118851783	1740391	0.00086	0.00001
1112.076	84335.6	327	111971322	1681075	0.00075	0.00001
1408.013	103327	325	170946707	2475788	0.00060	0.00009

Table 3.3: 16% HPGe detector efficiencies for ^{152}Eu decay energies at 13 cm
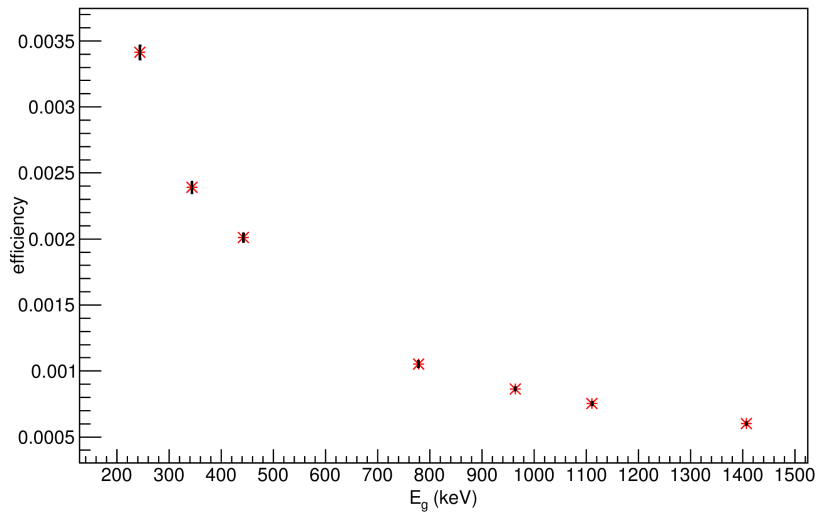
Figure 3.3: calibration curve of 16% HPGe detector at 13 cm

3.2 Reference foils' efficiency

The 16% HPGe detector's efficiencies at reference foils decay energies at 7 cm were determined using the ln(efficiency)=f(lnE$_\gamma$) graph (Fig. 3.4), which follows linear trend. For the error determination the 68% confidence level bands were designed in the same graph. The bands depict the upper and lower confidence bounds of all the points on the fitted line withing the range of data, and as a result the upper and the lower values of the respective efficiencies.
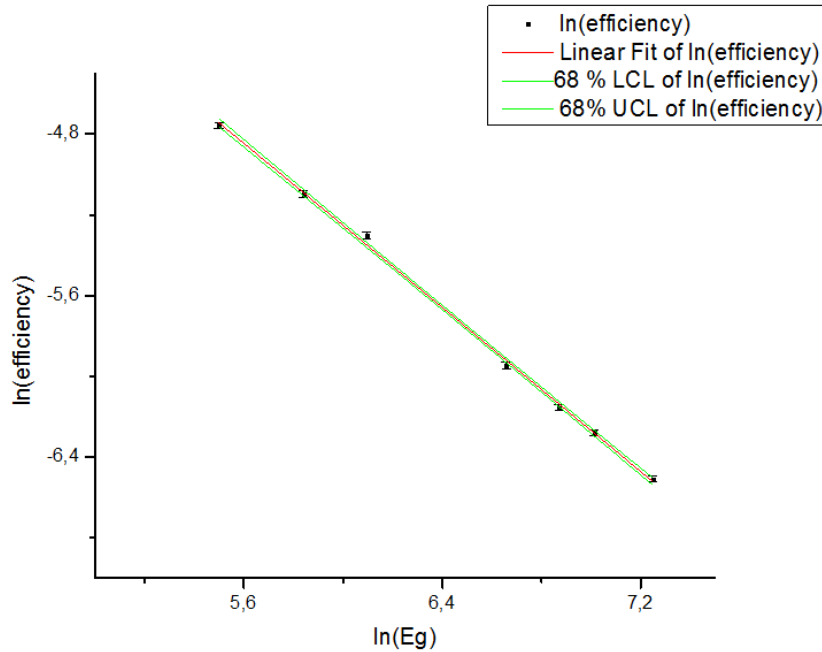
Figure 3.4: ln(efficiency)=f(lnEγ) graph for the 16% HPGe Detector at 7 cm.

From the above graph the following results accrued:

reference foils	daughter nuclei	decay energy (keV)	efficiency	$\sigma_{efficiency}$
^{27}Al	^{24}Na	1368.626	0.00151	0.00003
^{197}Au	^{196}Au	333.03	0.00636	0.0001
^{93}Nb	^{92m}Nb	934.44	0.00223	0.00003

Table 3.4: 16% HPGe detector efficiency for the reference foils' decay energies at 7 cm

3.3 2x100 % HPGe Detectors efficiency

[54]Mn Activity determination

As mentioned previously the 2x100% HPGe detectors were calibrated only for the [54]Mn decay energy at 834.8 keV. The problem with the [54]Mn point source was its unknown activity. To overcome this problem [54]Mn was placed at except for the 2x100 % HPGe detectors at the 16 % HPGe detector as well, at the distance of 13 cm from the detector's window.
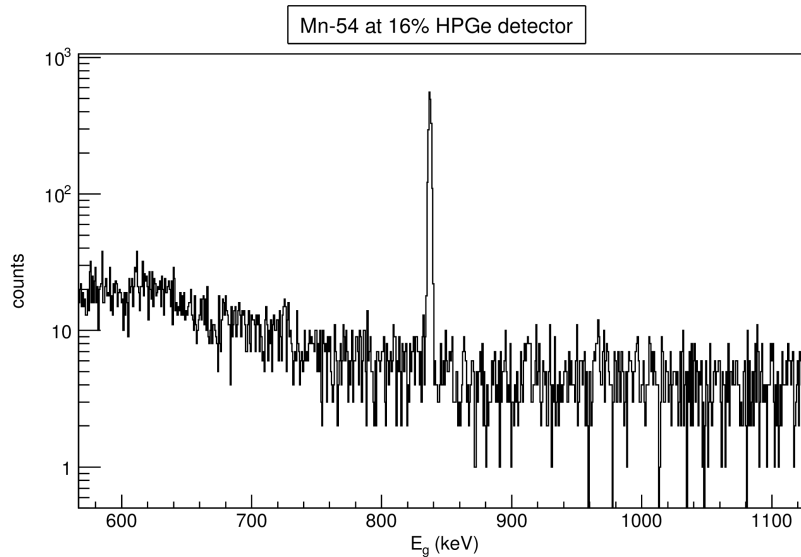
Figure 3.5: [54]Mn spectrum at 16% HPGe detector at 13 cm

The efficiency of the 16 % HPGe detector at 834.8 keV at 13 cm distance from the detector's window was calculated from the graph ln(efficiency)=f((lnEγ)) (Fig. 3.6) and was found equal to:

$$efficiency = \left(0.00100 \pm 0.00001\right)$$
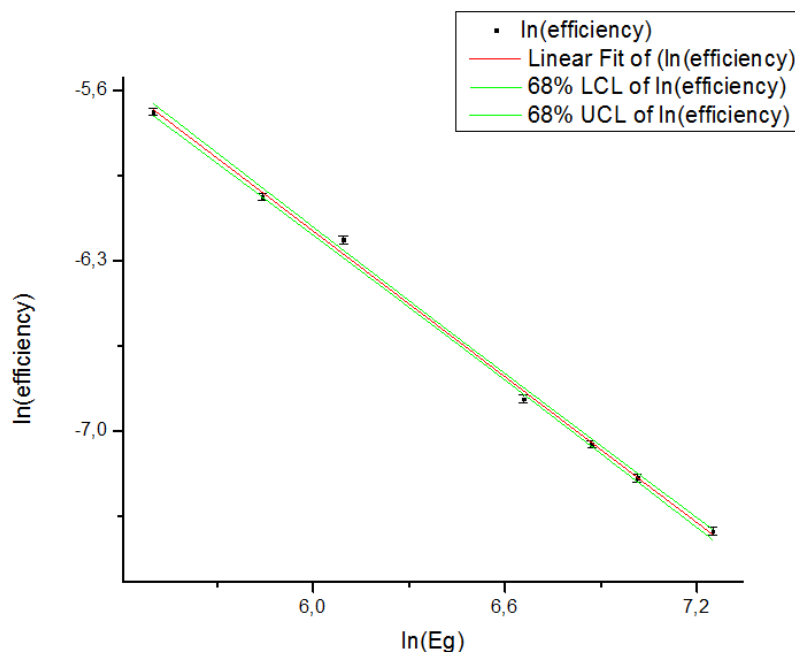
Figure 3.6: ln(efficiency)=f(lnEγ) graph for the 16% HPGe Detector at 13 cm

Since the efficiency and the counts of this decay energy were known, the respective emissions and , consequently, the ^{54}Mn source's activity could be determined via the equations :

$$emissions = \frac{counts}{efficiency} \ \ (eq\,3.4) \ \& \ \ Activity = \frac{emissions}{I\,live\,time} \ \ (eq.3.5)$$

- for detector's live-time=3599.682 s

Eɣ (keV)	efficiency	$\sigma_{efficiency}$	counts	σ_{counts}	emissions	$\sigma_{emissions}$	A (Bq)	σ_A (Bq)
834.848	0.00100	0.00001	1912	44	1907451	51647	530	14

Table 3.5: Mn-54 Activity determination

Finally, $A = (530 \pm 14)\,Bq$

^{54}Mn efficiency determination

After calculating the activity, the ^{54}Mn efficiency was calculated for each of the two 100% HPGe detectors separately, but also, for both of them by adding the separate spectra:

- first detector, $live\,time_1 = 4478.233\,s$:

Eɣ (keV)	counts	σ_{counts}	emissions	$\sigma_{emissions}$	efficiency	$\sigma_{efficiency}$
834.848	134012	368	2372990	64253	0.056	0.002

Table 3.6: efficiency determination of the first 100% HPGe detector at 834.848 keV energy at close geometry

- second detector, $live\,time_2 = 4480.267\,s$:

Eɣ (keV)	counts	σ_{counts}	emissions	$\sigma_{emissions}$	efficiency	$\sigma_{efficiency}$
834.848	117832	345	2374068	64282	0.050	0.001

Table 3.7: efficiency determination of the second 100% HPGe detector at 834.848 keV energy at close geometry

- both detectors, $live\,time = \dfrac{live\,time_1 + live\,time_2}{2} = 4479.25\,s$:

Eɣ (keV)	counts	σ_{counts}	emissions	$\sigma_{emissions}$	efficiency	$\sigma_{efficiency}$
834.848	252690	505	2373529	64268	0.106	0.003

Table 3.8: total efficiency for the 2x100% HPGe detectors at 834.848 keV energy at close geometry

3.4 Activity Measurements

3.4.1 Reference foils activity measurements

For the determination of the neutrons flux three reference reactions were used: ^{27}Al(n,a)^{24}Na , ^{197}Au(n,2n)^{196}Au and ^{93}Nb(n,2n)^{92m}Nb.

The information about details of the γ-ray activity measurements are given in this paragraph. Below some explanation with respect the used terminology is also given.

- live-time : the part of Data Acquisition Time (DAQ-Time) for which the detector electronics were active
- real-time: the actual DAQ-Time
- dead-time: the total time interval that DAQ system is busy for recording the detected pulses (real time-live time)
- waiting time: the time interval between the beam stop and the starting of γ-ray activity measurement

The final spectra were generated by adding the individual 1 hour spectra, which were recorded by the 16% HPGe detector. Respectively, the final real-times and live-times are the sum of the real-time and live-time of the added spectra.

Moreover, the graphs counts=f(real time) are presented. The graphs were fitted by the equation:

$$counts = A[0]\left(1 - e^{(-\lambda * real\,time)}\right) \quad \text{(eq. 3.6)}$$

where λ, the decay constant of the daughter nuclei

$$A[0] = efficiency\; I\; N_{act}\, e^{(-\lambda * waiting\,time)} \quad \text{(eq. 3.7)}$$

(Nact: the number of unstable nuclei at the stop of irradiation)

- first irradiation: E_n=10.7 MeV ➔ ^{27}Al(n,a)^{24}Na reference reaction

Figure 3.7: ^{24}Na spectrum at 16% HPGe Detector at 7 cm distance from the detector's window

- front Al-foil

measuring time (s)	28813
waiting time (s)	16967

Table 3.9: measuring and waiting time for the
Al front foil

spectra	real-time (s)	live-time (s)	counts	σ_{counts}	counts relative error
1st	3600	3599.824	243	16	0.07
2nd	7200	7199.623	490	23	0.05
3rd	10800	10799.403	718	28	0.04
4th	14400	14399.231	941	32	0.03
5th	18000	17999.004	1137	36	0.03
6th	21600	21598.78	1329	39	0.03
7th	25200	25198.584	1529	43	0.03
8th	28800	28798.393	1700	45	0.03

Table 3.10: the 16% HPGe detector real-times and live-times and the counts detected for the Al front foil
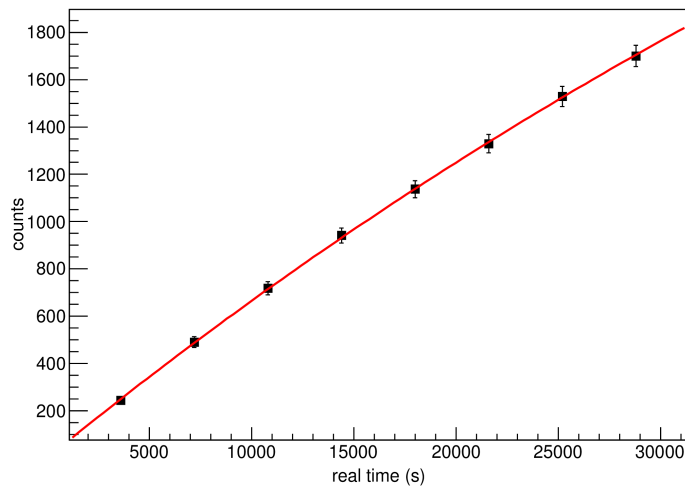
Figure 3.8: the counts=**f**(real time) graph for the Al front foil. The red line corresponds to
the expected growth of counts considering the half-life time of [24]Na

fitting parameter: $A[0] = (5517 \pm 66)$

- back Al-foil

measuring time (s)	14406
waiting time (s)	1961

Table 3.11 measuring and waiting time for the Al back foil

spectra	real-time (s)	live-time (s)	counts	σ_{counts}	counts relative error
1st	3600	3599.75	304	19	0.06
2nd	7200	7199.53	561	25	0.04
3rd	10800	10799.334	794	30	0.04
4th	14400	14399.123	1009	34	0.03

Table 3.12: 16% HPGe detector real-times and live-times and the counts detected for the Al back foil

Figure 3.9: the counts=**f**(real time) graph for the Al back foil. The red line corresponds to the expected growth of counts considering the half-life time of ^{24}Na

fitting parameter: $A[0]=6170\pm128$

- second irradiation: E_n=11.0 MeV → $^{97}Au(n,2n)^{196}Au$
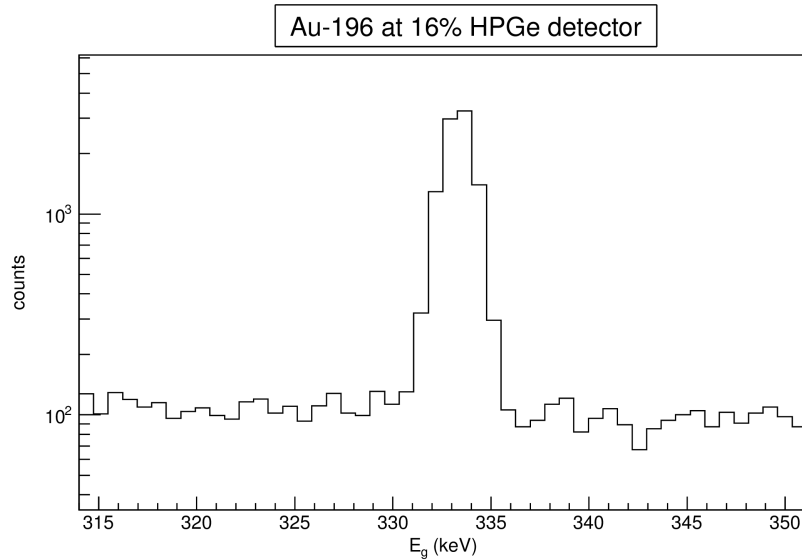
Figure 3.10: Part of the ^{196}Au spectrum at 16% HPGe Detector at 7 cm distance from the detector's window. The characteristic decay-line at 333.03 keV can be seen.

○ front Au-foil

measuring time (s)	3601
waiting time (s)	136450

Table 3.13: measuring and waiting time for the Au front foil

spectra	real-time (s)	live-time (s)	counts	σ_{counts}	counts relative error
1st	3600	3599.454	2609	56	0.02

Table 3.14: 16% HPGe detector real-times and live-times and the counts detected for the Au front foil

○ back Au-foil

measuring time (s)	14406
waiting time (s)	121311

Table 3.15: measuring and waiting time for the Au back foil

spectra	real time (s)	live time (s)	counts	σ_{counts}	counts relative error
1st	3600	3599.509	2335	52	0.02
2nd	7200	7198.984	4571	75	0.02
3rd	10800	10798.475	6828	91	0.01
4th	14400	14397.984	9060	104	0.01

Table 3.16: 16% HPGe detector real-times and live-times and the counts detected for the Au back foil
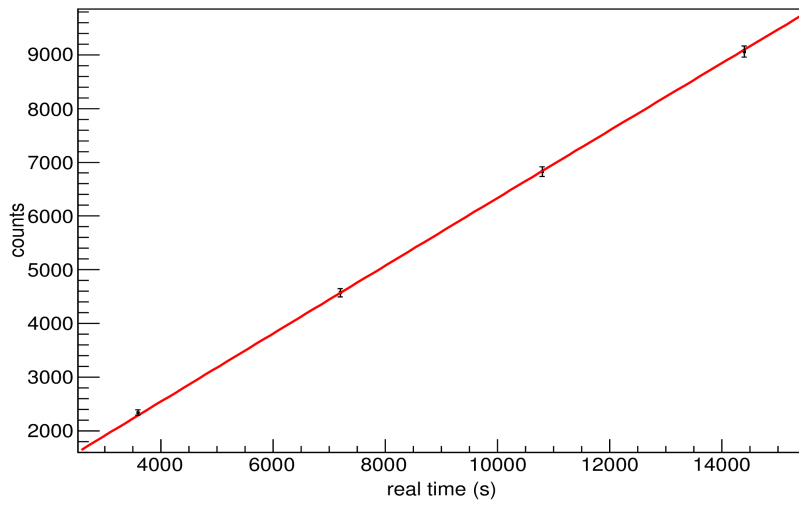
Figure 3.11: the counts=**f**(real time) graph for the Au back foil.The red line corresponds to the expected growth of counts considering the half-life time of ^{196}Au.

fitting parameter: A[0]= $\left(490149 \pm 3561\right)$
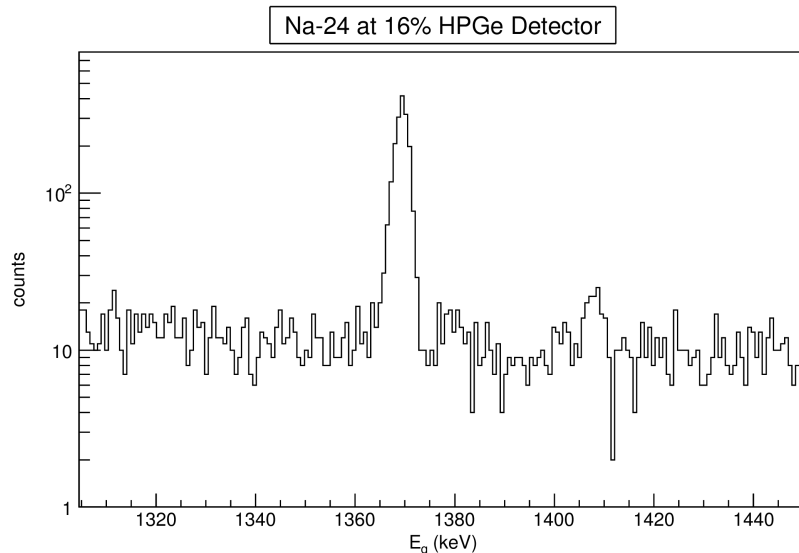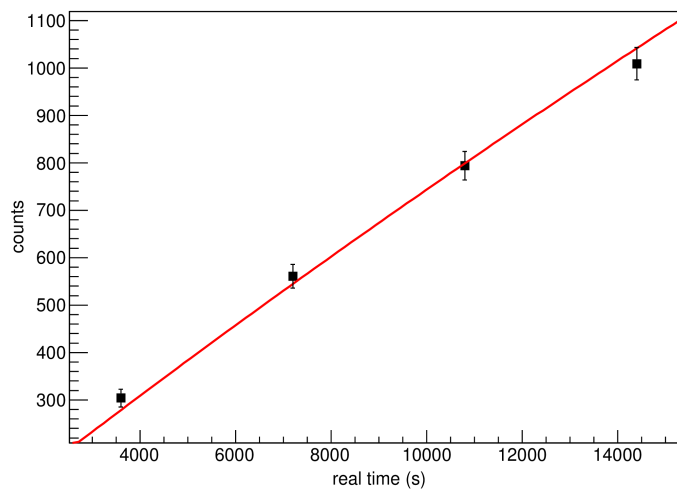
- third irradiation: En=11.3 MeV ➜ ^{93}Nb(n,2n)^{92m}Nb
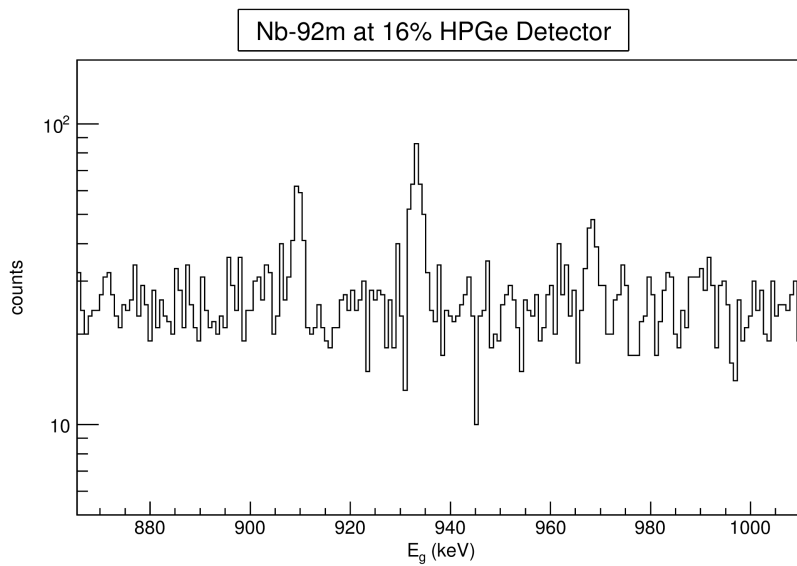
Figure 3.12: ^{92m}Nb spectrum at 16% HPGe Detector at 7 cm distance from the detector's window

○ front Nb-foil

measuring time (s)	18007
waiting time (s)	21293

Table 3.17: measuring and waiting time for the
Nb front foil

spectra	real-time (s)	live-time (s)	counts	σ_{counts}	counts relative error
1st	3600	3599.744	46	11	0.24
2nd	7200	7199.506	84	16	0.19
3rd	10800	10799.297	127	21	0.17
4th	14400	14399.064	180	27	0.15
5th	18000	17998.831	207	25	0.12

Table 3.18: the 16% HPGe detector real-times and live-times and the counts detected for the Nb front foil. The red line
corresponds to the expected growth of counts considering the half-life time of ^{92m}Nb
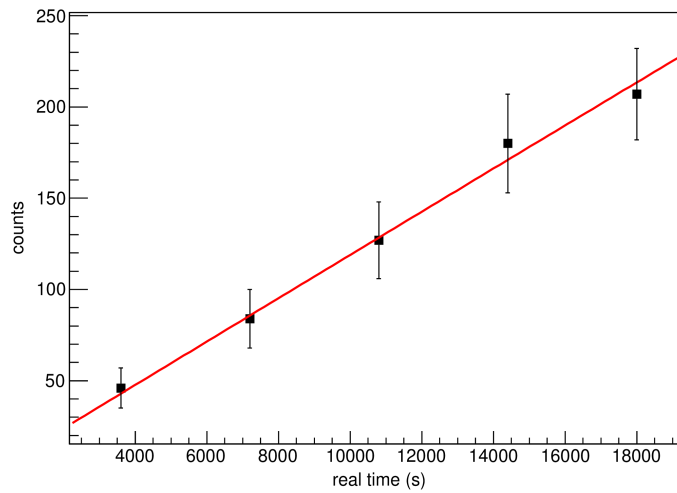
Figure 3.13: the counts=**f(**real time) graph for the Nb front foil

fitting parameter: $A[0]=(15117\pm1084)$

○ back Nb-foil

measuring time (s)	18439
waiting time (s)	2286

Table 3.19: measuring and waiting time for the
Nb back foil

spectra	real time (s)	live time (s)	counts	σ_{counts}	counts relative error
1st	3960.759	3960.462	54	11	0.20
2nd	7560.759	7560.209	93	15	0.16
3rd	11160.759	11159.984	144	18	0.13
4th	14760.759	14759.773	176	21	0.12
5th	1830.759	18359.563	211	25	0.12

Table 3.20: the 16% HPGe detector real-times and live-times and the counts detected for the Nb back foil
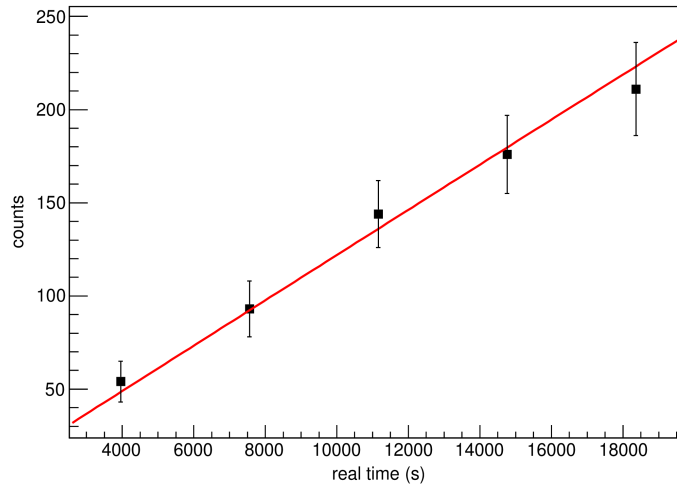
Figure 3.14: the counts=**f**(real time) graph for the Nb back foil. The red line corresponds
to the expected growth of counts considering the half-life time of ^{92m}Nb.

fitting parameter: $A[0]=(15499\pm948)$

3.4.2 ^{161}Er Activity

The decay rate of ^{161}Er was recorded following the counting rate of the most intense decay transition at 826.6 keV. The region of interest of the erbium sample γ-ray spectrum after 10 h of irradiation at 11.0 MeV neutron beam is presented at Figure 3.15. This spectrum resulted after 10 h of data acquisition. For the counts measurement the spectra of each 100% HPGe detector were added. For this reason before the measurement both detectors were very carefully gain matched.
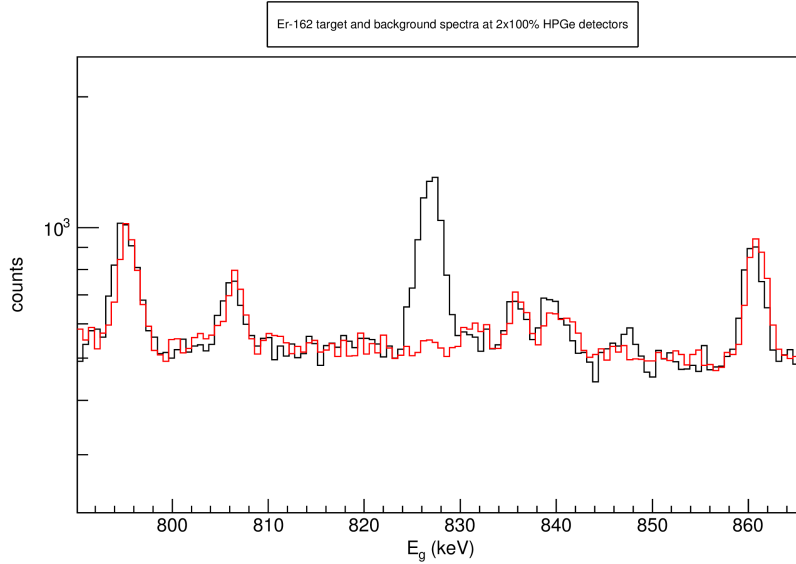
Figure 3.15: *^{162}Er target decay spectrum (black line) and the background spectrum (red line). The photopeak at 826.6 keV corresponds to the strongest decay γ-ray transition from the ^{161}Er decay*

Below the information about the recorded counts measuring time, the waiting time of measurement after the end of the irradiation and the counts measured are presented. Moreover the detectors' live-time and real-time are mentioned.

- first irradiation: E_n=10.7 MeV

measuring time (s)	14406
waiting time (s)	1961

Table 3.21: measuring and waiting time for the erbium target

spectra	real-time (s)	live-time (s)	counts	σ_{counts}	counts relative error
1st	3600	3597.245	144	29	0.20
2nd	7200	7194.4725	199	34	0.17
3rd	10800	10791.9495	289	46	0.16
4th	14400	13389.3745	324	52	0.16

Table 3.22: the 2x100% HPGe detectors real times and live times and the counts detected for the erbium target

Figure 3.16: the counts=f(real time) graph for the erbium target. The red line corresponds to the expected growth of counts considering the half-life time of ^{161}Er.

fitting parameter: $A[0] = (596 \pm 51)$

- second irradiation: $E_n = 11.0$ MeV

measuring time (s)	36378
waiting time (s)	1894

Table 3.23: measuring and waiting time for the erbium target

spectra	real-time (s)	live-time (s)	counts	σ_{counts}	counts relative error
1st	3600	3596.767	776	39	0.05
2nd	7200	7193.7445	1486	56	0.04
3rd	10800	10790.7935	1987	67	0.03
4th	14400	14387.892	2445	75	0.03
5th	18000	17985.068	2761	84	0.03
6th	21600	21582.2845	3113	91	0.03
7th	25200	25179.572	3295	98	0.03
8th	28800	28776.9005	3525	104	0.03
9th	32400	32374.28	3738	109	0.03
10th	36000	35971.67	3871	113	0.03

Table 3.24: the 2x100% HPGe detectors real-times and live-times and the counts detected for the erbium target
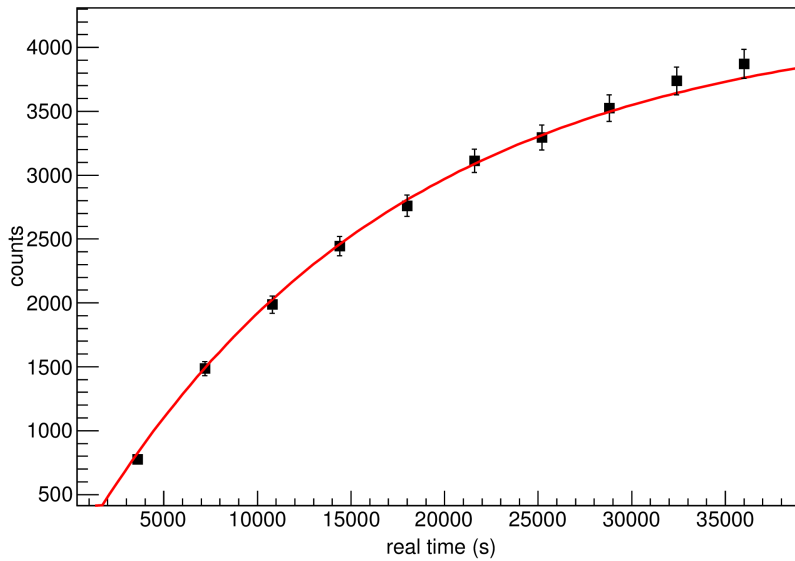
Table 3.17: the counts=**f**(real time) graph for the erbium target. The red line corresponds to the expected growth of counts considering the half-life time of ^{161}Er.

fitting parameter: $A[0]=(4252 \pm 43)$

- third irradiation: En=11.3 MeV

measuring time (s)	18439
waiting time (s)	2286

Table 3.25: measuring and waiting time for the erbium target

spectra	real-time (s)	live-time (s)	counts	σ_{counts}	counts relative error
1st	3960.759	3957.7745	271	35	0.13
2nd	7560.759	7555.25	306	39	0.13
3rd	11160.759	11152.764	405	47	0.12
4th	14760.759	14750.263	513	54	0.11
5th	18360.759	18347.734	574	60	0.10

Table 3.26: the 2x100% HPGe detectors real-times and live-times and the counts detected for the erbium target
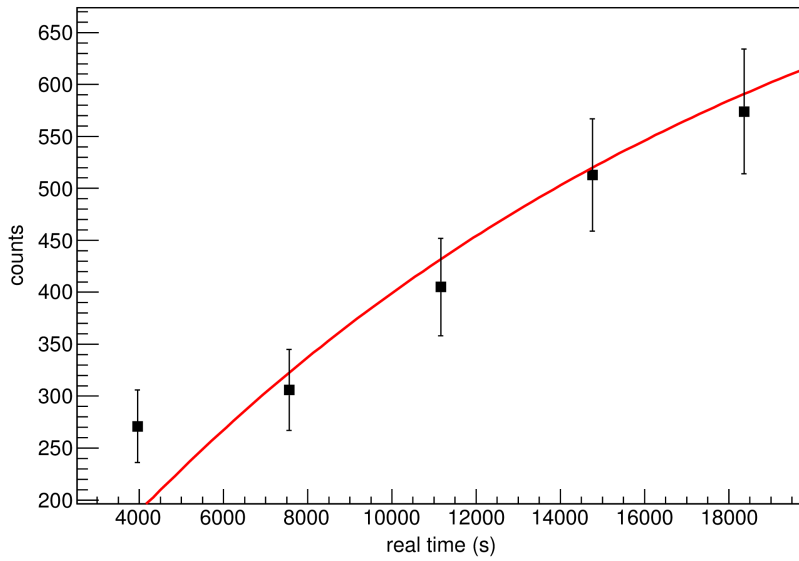
Figure 3.18: Table 18: the counts=f(real time) graph for the erbium target. The red line corresponds to the expected growth of counts considering the half-life time of ^{161}Er.

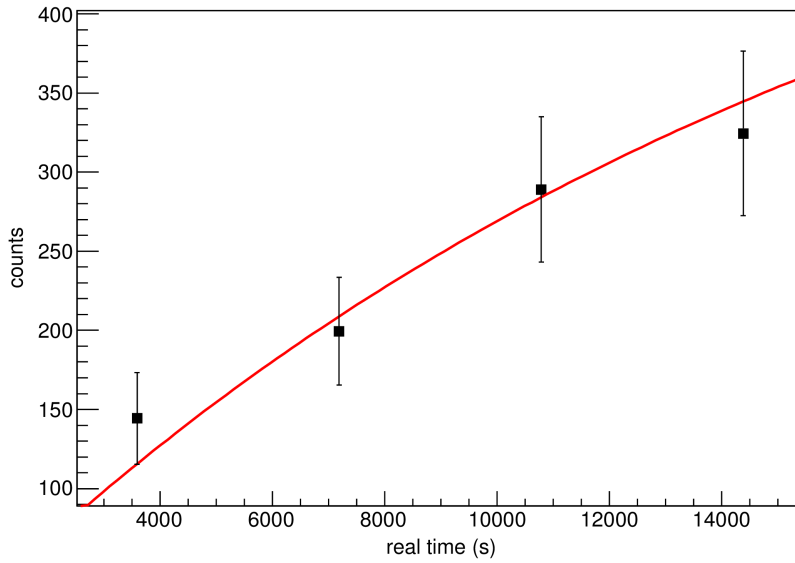fitting parameter: $A[0] = (885 \pm 46)$

3.5 Correction factors

3.5.1 Decay during irradiation correction factor

During the irradiations of the erbium sample unstable nuclei N_{act} (activated nuclei) were produced. Their rate of change is given from the equation:

$$\frac{dN_{act}}{dt} = \sigma f(t) N_T - \lambda N_{act} \quad \text{(eq. 3.9)}$$

where the first term describes the production of the activated nuclei and the second one their simultaneous decay.

The solution of the above differential equation is:

$$N_{act} = \sigma \Phi N_T f_b \quad \text{(eq. 3.10)}$$

where
$$f_b = \frac{\int_0^{t_{ir}} f(t) e^{\lambda t} dt}{\int_0^{t_{ir}} f(t) dt} e^{-\lambda t_{ir}} \quad \text{(eq. 3.11)}$$

calculates the balance between the activated nuclei that formed and them that decayed during the irradiation

Depending on whether the irradiation flux was constant or non-constant the f_b correction factor has two different solutions:

- for constant flux: $f(t) \rightarrow f_0$, the above equation has a simple analytical solution

$$f_b = \frac{(1 - e^{-\lambda t_{ir}})}{\lambda t_{ir}} \quad \text{(eq. 3.12)}$$

- for non-constant neutron flux the correction factor f_b becomes:

$$f_b = \frac{e^{-\lambda t_{ir}} \sum_{i=1} f_i (e^{(i+1)\lambda dt} - e^{i\lambda dt})}{\lambda dt \sum_{i=1} f_i} \quad \text{(eq. 3.13)}$$

Since the neutron flux was non-constant for the three irradiations at 10.7 MeV, 11.0 MeV and 11.3 MeV, a program has been developed at C++ programming language (see appendix B), which calculates the f_b correction factor in accordance with the above equation by taking into account the recorded neutron flux history files.

The f_b values for the erbium target and the reference foils are referred for each irradiation in the Table (3.27) :

first irradiation, E_n=10.7 MeV	
targets	f_b
^{162}Er	0.386853
^{27}Al	0.791465
second irradiation, E_n=11.0 MeV	
targets	f_b
^{162}Er	0.404055
^{197}Au	0.97669
third irradiation, E_n=11.3 MeV	
targets	f_b
^{162}Er	0.415989
^{93}Nb	0.985985

Table 3.27: f_b results as calculated for non-constant flux

The two correction factors referred below correct the fact that the counts detected are fewer than these the detectors should detect concerning their efficiency:

3.5.2 Self-Attenuation Correction factor

After the irradiation the number of activated nuclei is determined from the counting rate of the emitted γ-rays. A certain percentage of the emitted γ-rays is attenuated from the sample material and this has to be taken into account. For this reason the self-attenuation CF_{SA} correction factor has to be estimated.

$$total\,counts = CF_{SA} * detected\,counts \Rightarrow CF_{SA} = \frac{total\,counts}{detected\,counts} \quad \text{(eq. 3.14)}$$

where the total counts are the counts that would be detected supposing that there is no self-attenuation, i.e. the counts that would be detected in case the targets were point massless sources of γ-radiation.

In equivalence, the self-attenuation correction factor CF_{SA} can be expressed as the ratio of the detector's efficiency when the targets are point massless sources (ideal case) to the detector's efficiency when the targets are extended sources (actual case):

$$CF_{SA} = \frac{efficiency_{PS}}{efficiency_{ES}} \quad \text{(eq. 3.15)}$$

where efficiency$_{PS}$, the efficiency for point source
efficiency$_{ES}$, the efficiency for extended source

For the numerical determination of the terms efficiency$_{PS}$ and efficiency$_{ES}$ extended Geant4 Monte Carlo simulations were performed (see Appendix C). Firstly, the Geant4 MC simulations were tested by adopting the detector manufacturer geometrical specifications. The experimentally deduced detection efficiency was reproduced for several source to detector distances. Afterwards, the actual detection

geometry during the sample measurements was implemented in the Geant4 MC calculations for point source (PS) and for the extended source (ES).

source	E_γ (keV)	thickness (mm)	CF_{SA}	σ_{CF}
^{24}Na	1368.626	0.50	1.005	0.005
^{196}Au	333.03	0.50	1.128	0.002
^{92m}Nb	934.44	0.40	1.007	0.004

Table 3.28: the self-attenuation correction factors for the reference foils decay energies as estimated with the Geant4 MC calculations.

In the case of the erbium target the role of the CF_{SA} was dual: it does not only correct for the self-attenuation but also corrects for the fact that the 2x100% HPGe detectors were calibrated at 834.8 keV (^{54}Mn decay energy) and not at 826.6 keV which is the energy of the photons emitted during ^{161}Er decay:

$$\text{So for the erbium target:} \quad CF_{SA} = \frac{efficiency_{^{54}Mn}}{efficiency_{^{161}Er}} \quad \text{(eq. 3.16)}$$

where efficiency$_{54Mn}$ and efficiency$_{161Er}$ are the Geant4 code efficiency results for the ^{54}Mn point source and the erbium target (considering the real dimensions) respectively.

source	E_γ (keV)	thickness (mm)	CF_{SA}	σ_{CF}
^{161}Er	826.6	2	1.023	0.005

Table 3.29: the self- attenuation correction factor for the erbium target as estimated with the Geant4 MC calculations.

3.5.3 Dead-Time Correction factor

When a signal is recorded for a certain period of time the DAQ system is inactive. This time period corresponds to the needed time for signal processing and recording. This period of time (dead-time) for the total number of counts has to be taken into account. In this way the duration of measurement (real-time) is slightly different from the total time where the detector is actually active (live-time).

$$CF_{DT} = \frac{real\,time}{live\,time} \quad \text{(eq. 3.17)}$$

3.6 Reference reactions cross sections

The reference reactions cross sections were retrieved from the IRDFF data base [22]. In accordance to this:

En (MeV)	reference reaction	cross section (barns)	$\sigma_{\text{cross section}}$ (barns)
10.7	^{27}Al(n,α)^{24}Nα	0.102	0.001
	^{197}Au(n,2n)^{196}Au	1.35	0.04
	^{93}Nb(n,2n)^{92m}Nb	0.244	0.003
11.0	^{27}Al(n,α)^{24}Nα	0.106	0.001
	^{197}Au(n,2n)^{196}Au	1.45	0.04
	^{93}Nb(n,2n)^{92m}Nb	0.285	0.004
11.3	^{27}Al(n,α)^{24}Nα	0.109	0.001
	^{197}Au(n,2n)^{196}Au	1.55	0.04
	^{93}Nb(n,2n)^{92m}Nb	0.322	0.004

Table 3.30: the reference reactions cross section as retrieved from the IRDF v.1.05 data base.

3.7 Neutron Flux

The neutron flux during the erbium target irradiations was obtained from the mean value of the recorded neutron flux using the afore mentioned reference reactions. The monitor foils were placed front and back with respect the erbium target. The neutron flux uncertainty is 7% of the mean value:

$$\Phi = \frac{\Phi_{front} + \Phi_{back}}{2} \quad \text{(eq. 3.18)} \qquad \& \qquad \sigma_{\Phi} = 0.07\,\Phi \quad \text{(eq. 3.19)}$$

irradiation	foil	Φ (neutrons/cm²)
En=10.7 MeV	foil-front	1.37E+10
	foil-back	1.21E+10
En=11.0 MeV	foil-front	7.89E+10
	foil-back	7.11E+10
En=11.3 MeV	foil-front	1.10E+10
	foil-back	1.07E+10

Table 3.31: the neutrons fluxes at the front and back foils of the erbium target

The results of the integrated neutron flux at the erbium target are summarized in the Table 3.32:

E_n (MeV)	Φ (neutron/cm²)	σ_{Φ} (neutron/cm²)
10.7	1.29E+10	0.09E+10
11.0	7.50E+10	0.53E+10
11.3	1.09E+10	0.08E+10

Table 3.32: results for the integrated neutron flux at the erbium target

4. Results

As described previously the neutron flux was determined by recording the induced activity of the monitor foils according to the reference reactions. In this way all the parameters are known and the eq. 2.1 given below can be used as to deduce the reaction cross section:

$$\sigma = \frac{A\,CF_{SA}\,CF_{DT}}{N_T\,\Phi\,\varepsilon\,I_\gamma\left(1-e^{-\lambda t_m}\right)e^{-\lambda t_w}f_b}$$

The ^{162}Er(n,2n)^{161}Er reaction cross section at neutron energies of 10.7 MeV, 11.0 MeV and 11.3 MeV can be finally measured. The results are summarized in the Table 3.33. The graphical representation of the reaction cross section experimental results from the present work along with previous experimental results are presented in Fig. 3.19.

E_n (MeV)	cross section (barns)	$\sigma_{cross\ section}$ (barns)
10.7	0.44	0.08
11.0	0.56	0.06
11.3	0.71	0.10

Table 3.33: final cross section results
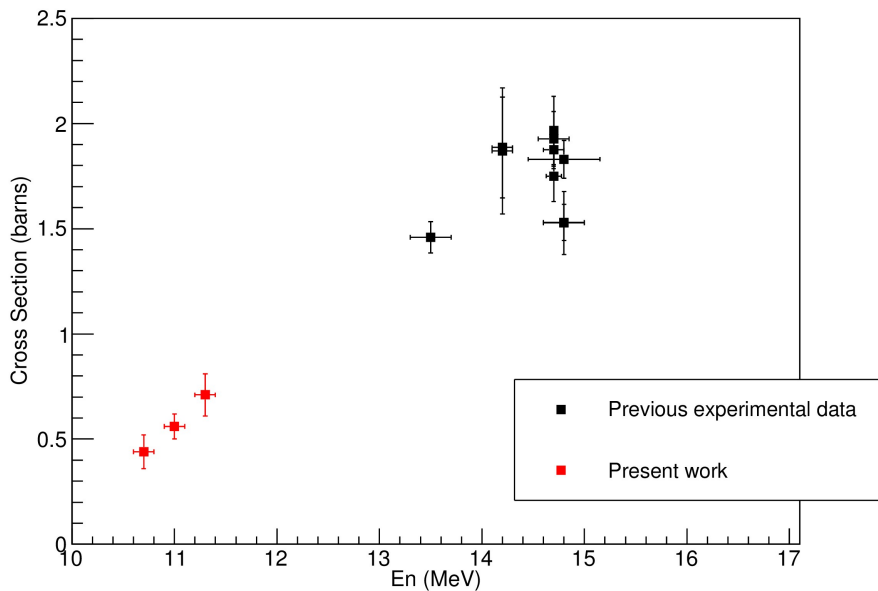
Figure 3.19: cross section graph for the ^{162}Er(n,2n)^{161}Er compound nucleus interaction

5. Conclusions

The ^{162}Er(n,2n)^{161}Er reaction cross section was measured for the first time at near threshold energies, at 10.7 MeV, 11.0 MeV and 11.3 MeV. The high sensitivity and the analytical power of the Activation Technique was important given that the abundance of ^{162}Er in the natural composition Erbium sample is only 0.139%. The minimal abundance of ^{162}Er in the sample was compensated by using an efficient 4π γ-ray detection set-up consisting of two 100 % relative efficiency HPGe detectors in close geometry. In future, the results of the present work along with the existing experimental data can be combined as to improve the "local" parameterization of the compound nucleus theoretical calculations. Furthermore, experimental data at higher neutron beam energies (e.g. E_n>17 MeV) are also needed as to map the excitation function.

Appendix A

The Cross Section equation

The formula which gives the cross section value in Activation Technique:

$$\sigma = \frac{counts}{\Phi\, I\, \varepsilon\, N_T\, e^{-\lambda t_w}\left(1 - e^{-\lambda t_m}\right) f_b}$$

is proven by combining the solution of the equation which describes the production of the unstable nuclei N_{act} with the solution of the equation which describes their decay.

- $\underline{N_{act}\ \text{production}}$

The production rate of the N_{act} nuclei is given by the formula:

$$\frac{d N_{act}}{dt} = \sigma f(t)\left(N_T - N_{act}\right) - \lambda N_{act}$$

where the term: $\sigma * f(t) * \left(N_T - N_{act}\right)$ describes their production during irradiation and the term $-\lambda N_{act}$ describes their simultaneous decay.

In equivalence: $\dfrac{dN_{act}}{dt} = \sigma f(t) N_T - \lambda N_{act}$, because $N_T - N_{act} \approx N_T$

The above differential equation has the following solution:

$$\frac{dN_{act}}{dt} = \sigma f(t) N_T - \lambda N_{act} \Longleftrightarrow$$

$$\frac{dN_{act}}{dt} e^{\lambda t} = \sigma f(t) N_T e^{\lambda t} - \lambda N_{act} e^{\lambda t} \Longleftrightarrow$$

$$\frac{dN_{act}}{dt} e^{\lambda t} + \lambda N_{act} e^{\lambda t} = \sigma f(t) N_T e^{\lambda t} \Longleftrightarrow$$

$$\frac{dN_{act}}{dt} e^{\lambda t} + N_{act} \frac{d e^{\lambda t}}{dt} = \sigma f(t) N_T e^{\lambda t} \Longleftrightarrow$$

$$d\frac{\left(N_{act}\,e^{\lambda t}\right)}{dt}=\sigma f(t)\,N_T\,e^{\lambda t}\Longleftrightarrow$$

By integrating from t=0 (start of irradiation, $N_{act}(0)=0$) until $t=t_{ir}$ (end of irradiation):

$$\int_0^{t_{ir}}d\frac{\left(N_{act}\,e^{\lambda t}\right)}{dt}\,dt=\int_0^{t_{ir}}\sigma f(t)\,N_T\,e^{\lambda t}\,dt\Longleftrightarrow$$

$$N_{act}\,e^{\lambda t_{ir}}=\int_0^{t_{ir}}\sigma f(t)\,N_T\,e^{\lambda t}\,dt\Longleftrightarrow$$

$$N_{act}=\frac{\sigma\,N_T\displaystyle\int_0^{t_{ir}}f(t)\,e^{\lambda t}\,dt}{e^{\lambda t_{ir}}}\Longleftrightarrow$$

$$N_{act}=\sigma\,N_T\left(\int_0^{t_{ir}}f(t)\,e^{\lambda t}\,dt\right)e^{-\lambda t}\Longleftrightarrow$$

$$N_{act}=\sigma\,N_T\left(\int_0^{t_{ir}}f(t)\,e^{\lambda t}\,dt\right)\frac{\displaystyle\int_0^{t_{ir}}f(t)\,dt}{\displaystyle\int_0^{t_{ir}}f(t)\,dt}\,e^{-\lambda t_{ir}}$$

The integral : $\displaystyle\int_0^{t_{ir}}f(t)\,dt$ is the total neutron flux Φ during the irradiation:

$$N_{act}=\sigma\,N_T\,\Phi\,e^{-\lambda t_{ir}}\frac{\displaystyle\int_0^{t_{irr}}f(t)\,e^{\lambda t}\,dt}{\displaystyle\int_0^{t_{ir}}f(t)\,dt}\Longleftrightarrow$$

$$N_{act} = \sigma N_T \Phi f_b \quad (1) \text{, where } \quad f_b = \frac{\int_0^{t_{ir}} f(t) e^{\lambda t} dt}{\int_0^{t_{ir}} f(t) dt} e^{-\lambda t_{ir}}$$

- N_act decay

The cps (counts per second) which the detector records are calculated via the formula:

$$cps = \frac{dN}{dt} \varepsilon I$$

$$cps = \lambda N \varepsilon I \Longleftrightarrow \qquad (\ \frac{dN}{dt} = \lambda N \ )$$

$$cps = \lambda N_0 e^{-\lambda t} \varepsilon I \Longleftrightarrow \qquad (\quad N = N_0 e^{-\lambda t} \ )$$

By integrating from t=0 (start measurement) until t=t_m (stop measurement):

$$counts = \int_0^{t_m} \left(\lambda N_0 e^{-\lambda t} \varepsilon I \right) dt \Longleftrightarrow$$

$$counts = \lambda \varepsilon I N_0 \int_0^{t_m} e^{-\lambda t} \Longleftrightarrow$$

$$counts = \varepsilon I N_0 \left(1 - e^{-\lambda t_m} \right)$$

where $\quad N_0 = N_{act} e^{-\lambda t_w}\quad$, as some N_act decayed after the end of the irradiation and before the detection start (waiting time).

$$\text{Finally,} \quad counts = \varepsilon I N_{act} e^{-\lambda t_w} \left(1 - e^{-\lambda t_m} \right) \quad (2)$$

By combining the equations (1) & (2) the cross section formula results:

$$\sigma = \frac{counts}{\Phi I \varepsilon N_T e^{-\lambda t_w} \left(1 - e^{-\lambda t_m} \right) f_b}$$

Appendix B

Decay during irradiation correction factor calculation program in C++ code

```cpp
# include <iostream>
# include <cmath>
# include <fstream>
using namespace std;

int main ()
{
  char   filename[20];
  double half_life;
  double lamda;
  double Irradiation_time;
  double dt;
  double flux[5000];
  double sum_1=0., sum_2=0.;
  int number_of_channels;
  cout<<"give the half life in seconds: ";
  cin>>half_life;
  lamda=log(2)/half_life;
  cout<<"give the name of the BF3 file: ";
  cin>>filename;
  cout<<"give the number of channels: ";
  cin>>number_of_channels;
  cout<<"give the dt of each channel: ";
  cin>>dt;
  Irradiation_time=number_of_channels*dt;
double fb;


ifstream infile;
infile.open(filename);
for (int i=0;i<number_of_channels;i++){
infile>>flux[i];
}
for(int j=0;j<number_of_channels;j++){
sum_2=sum_2+flux[j];
 sum_1=sum_1+flux[j]*(exp((j+1)*lamda*dt)-exp((j)*lamda*dt));
}
 fb=(exp(-lamda*Irradiation_time)/(lamda*dt))*(sum_1/sum_2);
cout<<"the correction factor for non constant flux is: ";
 cout<<fb<<"\n";
}
```

Appendix C

Geant4 MC simulation code for Self-Attenuation correction factor

The above Geant4 MC simulation code contains the geometry of the HPGe detector and the materials the [161]Er source consists of when it is extended and when it is assumed point.

```
//  Canberra Reverse-Electrode Coaxial Ge Detector GR 2018


#include "XriDetectorConstruction.hh"
#include "G4SDManager.hh"
#include "G4Element.hh"
#include "G4Material.hh"
#include "G4Box.hh"
#include "G4Tubs.hh"
#include "G4Cons.hh"
#include "G4LogicalVolume.hh"
#include "G4ThreeVector.hh"
#include "G4PVPlacement.hh"

#include "G4UnitsTable.hh"
#include "globals.hh"

#include "G4SystemOfUnits.hh"
#include "G4PhysicalConstants.hh"

#include "G4VisAttributes.hh"
#include "G4Colour.hh"

#include "G4SystemOfUnits.hh"
#include "G4PhysicalConstants.hh"

XriDetectorConstruction::XriDetectorConstruction()
{;}

XriDetectorConstruction::~XriDetectorConstruction()
{;}

G4VPhysicalVolume* XriDetectorConstruction::Construct()
{

  G4UnitDefinition::BuildUnitsTable();

    //=============================== materials
=====================================//

  G4double a;
  G4double z;
  G4int iz, in;
```

```cpp
  G4double density;
  G4String name, symbol;
  G4int ncomponents;
  G4double fractionmass;
  G4int natoms;

// ---------- plexiglass of Eu source

  a = 12.011*g/mole;
  G4Element* elC  = new G4Element(name="Carbon",symbol=" C" , z= 6., a);

  a = 1.008*g/mole;
  G4Element *elH  = new G4Element(name="Hydrogen",  symbol=" H" , z= 1., a);

  a = 15.999*g/mole;
  G4Element *elO  = new G4Element(name="Oxygen",  symbol=" O" , z= 8., a);

   // ERBIUM TARGET
    a=167.259*g/mole;

   G4Element *elEr  = new G4Element(name="Erbium",  symbol="Er" , z= 68., a);
  density = 8.64*g/cm3;
  G4Material* Er2O3 = new G4Material(name="Erbium_oxide",density,ncomponents=2);

  Er2O3->AddElement(elEr, natoms=2);
  Er2O3->AddElement(elO,  natoms=3);

  density = 1.5*g/cm3;
  G4Material* Cellulose = new G4Material("Cellulose" , density, ncomponents=3);
  Cellulose->AddElement(elH, natoms=10);
  Cellulose->AddElement(elC, natoms=6);
  Cellulose->AddElement(elO, natoms=5);

  density = 3.9*g/cm3;
  G4Material* ErTarget = new G4Material(name="ErTarget",density,ncomponents=2);
  ErTarget->AddMaterial(Cellulose,fractionmass=9.1*perCent);
  ErTarget->AddMaterial(Er2O3,fractionmass=90.9*perCent);

 /*  //POINT SOURCE
  density = 1.19*g/cm3;
  G4Material* Plexiglass = new G4Material(name="Plexiglass",density,ncomponents=3);
  Plexiglass->AddElement(elC, natoms=5);
  Plexiglass->AddElement(elH, natoms=8);
  Plexiglass->AddElement(elO, natoms=2); */



// -------  defining Ge crystal

  a = 72.61*g/mole;
  density = 5.323*g/cm3;
  G4Material* Ge = new G4Material(name="Ge",z=32., a, density);
```

```
// ------- defining Mg housing

  a = 24.305*g/mole;
  density = 1.738*g/cm3;
  G4Material* Mg = new G4Material(name="Mg", z=12., a, density);




// ------- defining Al housing

  a = 26.981539*g/mole;
  density = 2.70*g/cm3;
  G4Material* Al = new G4Material(name="Al", z=13., a, density);



//--------- defining Air

  a = 14.007*g/mole;
  G4Element* elN  = new G4Element(name="Nitrogen",symbol=" N" , z= 7., a);

// a = 15.999*g/mole;
// G4Element *elO  = new G4Element(name="Oxygen",  symbol=" O" , z= 8., a);

  density = 1.29*mg/cm3;
  G4Material *Air = new G4Material(name="Air ",density,ncomponents=2);
  Air->AddElement(elO, fractionmass=30.0*perCent);
  Air->AddElement(elN, fractionmass=70.0*perCent);

// -----   defining vacuum

  G4double pressure, temperature;
  density = universe_mean_density;
  pressure = 3.0E-18*pascal;
  temperature = 2.73*kelvin;
  G4Material *Vacuum = new G4Material(name="Vacuum", z=1.0, a=1.01*g/mole,
                       density, kStateGas, temperature, pressure);



  G4cout << "\n\n ####----------------------------------------------------#### \n";
  G4cout << "\n\t\t#### List of isotopes used #### \n";
// G4cout << *(G4Isotope::GetIsotopeTable());
  G4cout << "\n\n\n\n\t\t #### List of elements used #### \n";
  G4cout << *(G4Element::GetElementTable());
  G4cout << "\n\n\n\n\t\t #### List of materials used #### \n";
  G4cout << *(G4Material::GetMaterialTable());
  G4cout << "\n\n ####----------------------------------------------------#### \n";


      //================================= volumes =============================//

//---------------------------- beam line along z axis
```

```
   G4double startFi = 0.0*deg;
   G4double endFi = 360.0*deg;

//----------------------------- world volume

   G4double WorldOutR = 20.0*cm;
   G4double WorldInR = 0.0*cm;
   G4double WorldHalfh = 30.0*cm;

   G4Tubs *World_tub
     = new G4Tubs("World_tub",WorldInR,WorldOutR,WorldHalfh,
                              startFi,endFi);

   G4LogicalVolume *World_log
     = new G4LogicalVolume(World_tub,Air,"World_log",0,0,0);

   G4VPhysicalVolume *World_phys
     = new G4PVPlacement(0,G4ThreeVector(),"World",
                  World_log,0,false,0);


//--------------- Mg entrance window

   G4double SD = 1.75*cm;//1.75*cm;     // SD=Source-Detector distance, set equal to 7cm+0.5mm to the
source centre
   G4double MgWOutR = 4.5*cm;
   G4double MgWInR = 0.*cm;
   G4double MgWHalfh = (1.5/2)*mm;

   G4Tubs *MgW_tube
     = new G4Tubs("MgW_tube",MgWInR,MgWOutR,MgWHalfh,
                              startFi,endFi);

   G4LogicalVolume *MgW_log
     = new G4LogicalVolume(MgW_tube,Mg,"MgW_log",0,0,0);

   G4double Pos_x = 0.0*cm;
   G4double Pos_y = 0.0*cm;
   G4double Pos_z = -SD-MgWHalfh;
   G4VPhysicalVolume *MgWTube_phys
     = new G4PVPlacement(0,
          G4ThreeVector(Pos_x,Pos_y,Pos_z),
          MgW_log,"MgWTube",World_log,false,0);

//--------------- Mg entrance window 2


   G4LogicalVolume *MgW_log2
   = new G4LogicalVolume(MgW_tube,Mg,"MgW_log2",0,0,0);

   Pos_x = 0.0*cm;
```

```
  Pos_y = 0.0*cm;
  Pos_z = SD+MgWHalfh;
  G4VPhysicalVolume *MgWTube_phys2
   = new G4PVPlacement(0,
        G4ThreeVector(Pos_x,Pos_y,Pos_z),
          MgW_log2,"MgWTube2",World_log,false,0);



//----------------- Mg housing

  G4double MgThickness = 1.5*mm;
  G4double MgOutR = MgWOutR;
  G4double MgInR = 0.*cm;
  G4double MgHalfh = (16.4/2.)*cm;

  G4Tubs *Mg_tube
    = new G4Tubs("Mg_tube",MgInR,MgOutR,MgHalfh,
                            startFi,endFi);

  G4LogicalVolume *Mg_log
    = new G4LogicalVolume(Mg_tube,Mg,"Mg_log",0,0,0);

  Pos_x = 0.0*cm;
  Pos_y = 0.0*cm;
  Pos_z = -SD-2.*MgWHalfh-MgHalfh;
  G4VPhysicalVolume *MgTube_phys
   = new G4PVPlacement(0,
        G4ThreeVector(Pos_x,Pos_y,Pos_z),
        Mg_log,"MgTube",World_log,false,0);

//----------------- Mg housing 2

  G4LogicalVolume *Mg_log2
    = new G4LogicalVolume(Mg_tube,Mg,"Mg_log2",0,0,0);

  Pos_x = 0.0*cm;
  Pos_y = 0.0*cm;
  Pos_z = SD+2.*MgWHalfh+MgHalfh;
  G4VPhysicalVolume *MgTube_phys2
   = new G4PVPlacement(0,
        G4ThreeVector(Pos_x,Pos_y,Pos_z),
        Mg_log2,"MgTube2",World_log,false,0);



//-------------- Vacuum between Mg window and Mg housing

  G4double VacuumOutR = MgOutR - MgThickness;
  G4double VacuumInR = 0.*cm;
  G4double VacuumHalfh = MgHalfh - MgThickness/2.;
```

```cpp
  G4Tubs *Vacuum_tube
    = new G4Tubs("Vacuum_tube",VacuumInR,VacuumOutR,VacuumHalfh,
                              startFi,endFi);

  G4LogicalVolume *Vacuum_log
    = new G4LogicalVolume(Vacuum_tube,Vacuum,"Vacuum_log",0,0,0);

  Pos_x = 0.0*cm;
  Pos_y = 0.0*cm;
  Pos_z = MgThickness/2.;
  G4VPhysicalVolume *VacuumTube_phys
    = new G4PVPlacement(0,
          G4ThreeVector(Pos_x,Pos_y,Pos_z),
          Vacuum_log,"VacuumTube",Mg_log,false,0);

//-------------- Vacuum between Mg window2 and Mg housing2


  G4LogicalVolume *Vacuum_log2
    = new G4LogicalVolume(Vacuum_tube,Vacuum,"Vacuum_log2",0,0,0);

  Pos_x = 0.0*cm;
  Pos_y = 0.0*cm;
  Pos_z = -MgThickness/2.;
  G4VPhysicalVolume *VacuumTube_phys2
    = new G4PVPlacement(0,
          G4ThreeVector(Pos_x,Pos_y,Pos_z),
          Vacuum_log2,"VacuumTube2",Mg_log2,false,0);

//--------------- Al mylar entrance window

  G4double gapMg_Al = 3.95*mm;
  G4double AlWOutR = 3.956*cm;
  G4double AlWInR = 0.*cm;
  G4double AlWHalfh = (0.05/2)*mm;

  G4Tubs *AlW_tube
    = new G4Tubs("AlW_tube",AlWInR,AlWOutR,AlWHalfh,
                              startFi,endFi);

  G4LogicalVolume *AlW_log
    = new G4LogicalVolume(AlW_tube,Al,"AlW_log",0,0,0);

  Pos_x = 0.0*cm;
  Pos_y = 0.0*cm;
  Pos_z = VacuumHalfh-gapMg_Al-AlWHalfh;
  G4VPhysicalVolume *AlWTube_phys
    = new G4PVPlacement(0,
          G4ThreeVector(Pos_x,Pos_y,Pos_z),
          AlW_log,"AlWTube",Vacuum_log,false,0);
```

```
//-------------- Al mylar entrance window2


  G4LogicalVolume *AlW_log2
    = new G4LogicalVolume(AlW_tube,Al,"AlW_log2",0,0,0);

  Pos_x = 0.0*cm;
  Pos_y = 0.0*cm;
  Pos_z = -(VacuumHalfh-gapMg_Al-AlWHalfh);
  G4VPhysicalVolume *AlWTube_phys2
    = new G4PVPlacement(0,
         G4ThreeVector(Pos_x,Pos_y,Pos_z),
         AlW_log2,"AlWTube2",Vacuum_log2,false,0);


//----------------- Al housing

  G4double AlThickness = 0.76*mm;
  G4double AlOutR = AlWOutR;
  G4double AlInR = 0.*cm;
  G4double AlHalfh = (12.68/2.)*cm;

  G4Tubs *Al_tube
    = new G4Tubs("Al_tube",AlInR,AlOutR,AlHalfh,
                              startFi,endFi);

  G4LogicalVolume *Al_log
    = new G4LogicalVolume(Al_tube,Al,"Al_log",0,0,0);

  Pos_x = 0.0*cm;
  Pos_y = 0.0*cm;
  Pos_z = VacuumHalfh-gapMg_Al-2*AlWHalfh - AlHalfh;
  G4VPhysicalVolume *AlTube_phys
    = new G4PVPlacement(0,
         G4ThreeVector(Pos_x,Pos_y,Pos_z),
         Al_log,"AlTube",Vacuum_log,false,0);

//----------------- Al housing2


  G4LogicalVolume *Al_log2
    = new G4LogicalVolume(Al_tube,Al,"Al_log2",0,0,0);

  Pos_x = 0.0*cm;
  Pos_y = 0.0*cm;
  Pos_z = -(VacuumHalfh-gapMg_Al-2*AlWHalfh - AlHalfh);
  G4VPhysicalVolume *AlTube_phys2
    = new G4PVPlacement(0,
         G4ThreeVector(Pos_x,Pos_y,Pos_z),
         Al_log2,"AlTube2",Vacuum_log2,false,0);
```

```
//------------- Vacuum between Al  window and Al housing

  G4double InVacuumOutR = AlOutR - AlThickness;
  G4double InVacuumInR = 0.*cm;
  G4double InVacuumHalfh = AlHalfh - AlThickness/2.;

  G4Tubs *InVacuum_tube
    = new G4Tubs("InVacuum_tube",InVacuumInR,InVacuumOutR,InVacuumHalfh,
                          startFi,endFi);

  G4LogicalVolume *InVacuum_log
    = new G4LogicalVolume(InVacuum_tube,Vacuum,"InVacuum_log",0,0,0);

  Pos_x = 0.0*cm;
  Pos_y = 0.0*cm;
  Pos_z = AlThickness/2.;
  G4VPhysicalVolume *InVacuumTube_phys
    = new G4PVPlacement(0,
          G4ThreeVector(Pos_x,Pos_y,Pos_z),
          InVacuum_log,"InVacuumTube",Al_log,false,0);


//------------- Vacuum between Al  window2  and Al housing2


  G4LogicalVolume *InVacuum_log2
    = new G4LogicalVolume(InVacuum_tube,Vacuum,"InVacuum_log2",0,0,0);

  Pos_x = 0.0*cm;
  Pos_y = 0.0*cm;
  Pos_z = -AlThickness/2.;
  G4VPhysicalVolume *InVacuumTube_phys2
    = new G4PVPlacement(0,
          G4ThreeVector(Pos_x,Pos_y,Pos_z),
          InVacuum_log2,"InVacuumTube2",Al_log2,false,0);


//------------- Dead layer Window Ge cone front


  G4double FDLWConeRadiusUpMax = 3.58 *cm; //Front Dead Layer Window Uppper Max Radius
  G4double FDLWConeRadiusUpMin = 0.0 *cm; //Front Dead Layer Window Uppper Min Radius
  G4double FDLWConeRadiusBottomMax = 3.68 *cm; //Front Dead Layer Window Bottom Max Radius
  G4double FDLWConeRadiusBottomMin = 0.0 *cm; //Front Dead Layer Window Bottom Min Radius
  G4double FDLWConeHalfHeight = (0.00003/2.0)*cm; //Front Dead Layer thinkness

  G4Cons *FDLW_cone
    = new G4Cons("FDLW_cone", FDLWConeRadiusBottomMin, FDLWConeRadiusBottomMax,
                    FDLWConeRadiusUpMin,FDLWConeRadiusUpMax,
                    FDLWConeHalfHeight,
                startFi,endFi);
```

```
G4LogicalVolume *FDLW_log
  = new G4LogicalVolume(FDLW_cone,Ge,"FDLW_log",0,0,0);


Pos_x = 0.0*cm;
Pos_y = 0.0*cm;
Pos_z = InVacuumHalfh-FDLWConeHalfHeight;
G4VPhysicalVolume *FDLWCone_phys
  = new G4PVPlacement(0,
        G4ThreeVector(Pos_x,Pos_y,Pos_z),
        FDLW_log,"FDLWCone",InVacuum_log,false,0);



//-------------- Dead layer Window2 Ge cone front

G4double FDLWConeRadiusUpMax2 = 3.68 *cm; //Front Dead Layer Window Uppper Max Radius
G4double FDLWConeRadiusUpMin2 = 0.0 *cm; //Front Dead Layer Window Uppper Min Radius
G4double FDLWConeRadiusBottomMax2 = 3.58 *cm; //Front Dead Layer Window Bottom Max Radius
G4double FDLWConeRadiusBottomMin2 = 0.0 *cm; //Front Dead Layer Window Bottom Min Radius
G4double FDLWConeHalfHeight2 = (0.00003/2.0)*cm; //Front Dead Layer thinkness

G4Cons *FDLW_cone2
  = new G4Cons("FDLW_cone2", FDLWConeRadiusBottomMin2, FDLWConeRadiusBottomMax2,
                    FDLWConeRadiusUpMin2,FDLWConeRadiusUpMax2,
                    FDLWConeHalfHeight2,
              startFi,endFi);



G4LogicalVolume *FDLW_log2
  = new G4LogicalVolume(FDLW_cone2,Ge,"FDLW_log2",0,0,0);

Pos_x = 0.0*cm;
Pos_y = 0.0*cm;
Pos_z = -(InVacuumHalfh-FDLWConeHalfHeight2);
G4VPhysicalVolume *FDLWCone_phys2
  = new G4PVPlacement(0,
        G4ThreeVector(Pos_x,Pos_y,Pos_z),
        FDLW_log2,"FDLWCone2",InVacuum_log2,false,0);


//-------------- Front Ge cone


G4double FrontGeConeRadiusUpMax = 3.68 *cm; // Ge cone upper max radius
G4double FrontGeConeRadiusUpMin = 0.0 *cm; // Ge cone upper min radius
G4double FrontGeConeRadiusBottomMax = 3.78 *cm; // Ge cone bottom max radius
G4double FrontGeConeRadiusBottomMin = 0.0 *cm; // Ge cone bottom min radius
G4double FrontGeConeHalfHeight = (0.1/2.0)*cm; //Front Dead Layer thinkness
```

```
  G4Cons *frontGe_cone
    = new G4Cons("frontGe_cone",FrontGeConeRadiusBottomMin, FrontGeConeRadiusBottomMax,
                      FrontGeConeRadiusUpMin,FrontGeConeRadiusUpMax,
                      FrontGeConeHalfHeight,
                  startFi,endFi);


  G4LogicalVolume *frontGeCone_log
    = new G4LogicalVolume(frontGe_cone,Ge,"frontGeCone_log",0,0,0);


  Pos_x = 0.0*cm;
  Pos_y = 0.0*cm;
  Pos_z = InVacuumHalfh-2*FDLWConeHalfHeight-FrontGeConeHalfHeight;
  G4VPhysicalVolume *frontGeCone_phys
    = new G4PVPlacement(0,
         G4ThreeVector(Pos_x,Pos_y,Pos_z),
         frontGeCone_log,"frontGeCone",InVacuum_log,false,0);

//-------------- Front Ge cone2

  G4double FrontGeConeRadiusUpMax2 = 3.78 *cm; // Ge cone upper max radius
  G4double FrontGeConeRadiusUpMin2 = 0.0 *cm; // Ge cone upper min radius
  G4double FrontGeConeRadiusBottomMax2 = 3.68 *cm; // Ge cone bottom max radius
  G4double FrontGeConeRadiusBottomMin2 = 0.0 *cm; // Ge cone bottom min radius
  G4double FrontGeConeHalfHeight2 = (0.1/2.0)*cm; //Front Dead Layer thinkness

  G4Cons *frontGe_cone2
    = new G4Cons("frontGe_cone2",FrontGeConeRadiusBottomMin2, FrontGeConeRadiusBottomMax2,
                      FrontGeConeRadiusUpMin2,FrontGeConeRadiusUpMax2,
                      FrontGeConeHalfHeight2,
                  startFi,endFi);

   G4LogicalVolume *frontGeCone_log2
    = new G4LogicalVolume(frontGe_cone2,Ge,"frontGeCone_log2",0,0,0);


  Pos_x = 0.0*cm;
  Pos_y = 0.0*cm;
  Pos_z = -(InVacuumHalfh-2*FDLWConeHalfHeight2-FrontGeConeHalfHeight2);
  G4VPhysicalVolume *frontGeCone_phys2
    = new G4PVPlacement(0,
         G4ThreeVector(Pos_x,Pos_y,Pos_z),
         frontGeCone_log2,"frontGeCone2",InVacuum_log2,false,0);

// ----------- Plexiglass or target

  G4double PlexiOutR = 1.295/2.*cm;//2.0/2.*cm;
  G4double PlexiInR = 0.*cm;
  G4double PlexiHalfh = 0.2/2.*cm;

  G4Tubs *Plexi_tube
    = new G4Tubs("Plexi_tube",PlexiInR,PlexiOutR,PlexiHalfh,
                           startFi,endFi);
```

```
G4LogicalVolume *Plexi_log
  = new G4LogicalVolume(Plexi_tube,ErTarget,"Plexi_log",0,0,0);


Pos_x = 0.0*cm;
Pos_y = 0.0*cm;
Pos_z = 0.0*cm; //Here Christine had:    -PlexiHalfh/2.;
G4VPhysicalVolume *PlexiTube_phys
  = new G4PVPlacement(0,
        G4ThreeVector(Pos_x,Pos_y,Pos_z),
        Plexi_log,"PlexiTube",World_log,false,0);



//------------- Dead layer of crystal at the crystal sides: denoted as "outDead"


  G4double GeOutR = 3.77997*cm;  //***HTAN 50/2*
  G4double GeHalfh = 8.99/2.*cm;
  G4double outDeadThickness = 0.00003*cm;
  G4double outDeadOutR = GeOutR + outDeadThickness;
  G4double outDeadInR = 0.*mm;
  G4double outDeadHalfh = GeHalfh;

  G4Tubs *outDead_tube
    = new G4Tubs("outDead_tube",outDeadInR,outDeadOutR,outDeadHalfh,
                            startFi,endFi);

  G4LogicalVolume *outDead_log
    = new G4LogicalVolume(outDead_tube,Ge,"outDead_log",0,0,0);

  Pos_x = 0.0*cm;
  Pos_y = 0.0*cm;
  Pos_z =InVacuumHalfh-2*FDLWConeHalfHeight-2*FrontGeConeHalfHeight-outDeadHalfh;

  G4VPhysicalVolume *outDeadTube_phys
   = new G4PVPlacement(0,
        G4ThreeVector(Pos_x,Pos_y,Pos_z),
        outDead_log,"outDeadTube",InVacuum_log,false,0);



//------------- Dead layer 2  of crystal at the crystal sides: denoted as "outDead2"


  G4LogicalVolume *outDead_log2
  = new G4LogicalVolume(outDead_tube,Ge,"outDead_log2",0,0,0);

  Pos_x = 0.0*cm;
  Pos_y = 0.0*cm;
  Pos_z =-(InVacuumHalfh-2*FDLWConeHalfHeight2-2*FrontGeConeHalfHeight2-outDeadHalfh);
```

```
  G4VPhysicalVolume *outDeadTube_phys2
   = new G4PVPlacement(0,
         G4ThreeVector(Pos_x,Pos_y,Pos_z),
         outDead_log2,"outDeadTube2",InVacuum_log2,false,0);



//----------------- Ge crystal

  G4double GeInR = 0.*mm;

  G4Tubs *Ge_tube
    = new G4Tubs("Ge_tube",GeInR,GeOutR,GeHalfh,
                              startFi,endFi);

  G4LogicalVolume *Ge_log
    = new G4LogicalVolume(Ge_tube,Ge,"Ge_log",0,0,0);

  Pos_x = 0.0*cm;
  Pos_y = 0.0*cm;
  Pos_z = 0.0*cm;
  G4VPhysicalVolume *GeTube_phys
    = new G4PVPlacement(0,
         G4ThreeVector(Pos_x,Pos_y,Pos_z),
         Ge_log,"GeTube",outDead_log,false,0);

//----------------- Ge crystal 2


  G4LogicalVolume *Ge_log2
   = new G4LogicalVolume(Ge_tube,Ge,"Ge_log2",0,0,0);

  Pos_x = 0.0*cm;
  Pos_y = 0.0*cm;
  Pos_z = 0.0*cm;
  G4VPhysicalVolume *GeTube_phys2
   = new G4PVPlacement(0,
         G4ThreeVector(Pos_x,Pos_y,Pos_z),
         Ge_log2,"GeTube2",outDead_log2,false,0);

//----------- Dead layer in borehole: denoted as inDead

  G4double BoreholeHalfh = 84/2.*mm;
  G4double BoreholeOutR = 10.1/2.*mm;
  G4double inDeadThickness =0.7*mm;
  G4double inDeadOutR = BoreholeOutR + inDeadThickness;
  G4double inDeadInR = 0.*mm;
  G4double inDeadHalfh = BoreholeHalfh + inDeadThickness/2.;

  G4Tubs *inDead_tube
    = new G4Tubs("inDead_tube",inDeadInR,inDeadOutR,inDeadHalfh,
                              startFi,endFi);
```

```
G4LogicalVolume *inDead_log
  = new G4LogicalVolume(inDead_tube,Ge,"inDead_log",0,0,0);


Pos_x = 0.0*cm;
Pos_y = 0.0*cm;
Pos_z = - GeHalfh + inDeadHalfh;
G4VPhysicalVolume *inDeadTube_phys
  = new G4PVPlacement(0,
      G4ThreeVector(Pos_x,Pos_y,Pos_z),
      inDead_log,"inDeadTube",Ge_log,false,0);




//----------- Dead layer 2 in borehole 2: denoted as inDead2


G4LogicalVolume *inDead_log2
  = new G4LogicalVolume(inDead_tube,Ge,"inDead_log2",0,0,0);


Pos_x = 0.0*cm;
Pos_y = 0.0*cm;
Pos_z = -(- GeHalfh + inDeadHalfh);
G4VPhysicalVolume *inDeadTube_phys2
  = new G4PVPlacement(0,
      G4ThreeVector(Pos_x,Pos_y,Pos_z),
      inDead_log2,"inDeadTube2",Ge_log2,false,0);

//-------------- Borehole

G4double BoreholeInR = 0.*mm;

G4Tubs *Borehole_tube
  = new G4Tubs("Borehole_tube",BoreholeInR,BoreholeOutR,BoreholeHalfh,
                            startFi,endFi);

G4LogicalVolume *Borehole_log
  = new G4LogicalVolume(Borehole_tube,Vacuum,"Borehole_log",0,0,0);


Pos_x = 0.0*cm;
Pos_y = 0.0*cm;
Pos_z = - inDeadThickness/2.;
G4VPhysicalVolume *BoreholeTube_phys
  = new G4PVPlacement(0,
      G4ThreeVector(Pos_x,Pos_y,Pos_z),
      Borehole_log,"BoreholeTube",inDead_log,false,0);


//-------------- Borehole 2


G4LogicalVolume *Borehole_log2
  = new G4LogicalVolume(Borehole_tube,Vacuum,"Borehole_log2",0,0,0);
```

```
Pos_x = 0.0*cm;
Pos_y = 0.0*cm;
Pos_z =-(- inDeadThickness/2.);
G4VPhysicalVolume *BoreholeTube_phys2
  = new G4PVPlacement(0,
       G4ThreeVector(Pos_x,Pos_y,Pos_z),
       Borehole_log2,"BoreholeTube2",inDead_log2,false,0);




    //======================= Visualization attributes
=======================================//

  World_log->SetVisAttributes (G4VisAttributes::Invisible);
  G4VisAttributes *MgWTubeAttr = new G4VisAttributes(G4Colour(0.,0.,1.));       //Blue
  G4VisAttributes *AlWTubeAttr = new G4VisAttributes(G4Colour(0.,0.,1.));       //Blue
  G4VisAttributes *MgTubeAttr = new G4VisAttributes(G4Colour(1.,0.,0.));       //Red

G4VisAttributes *AlTubeAttr = new G4VisAttributes(G4Colour(1.,0.,0.));       //Red
  G4VisAttributes *VacuumTubeAttr = new G4VisAttributes(G4Colour(0.3,0.3,0.3)); //light gray
 G4VisAttributes *InVacuumTubeAttr = new G4VisAttributes(G4Colour(0.3,0.3,0.3)); //light gray
  G4VisAttributes *outDeadTubeAttr = new G4VisAttributes(G4Colour(0.,1.,0.));    //green
  G4VisAttributes *GeTubeAttr = new G4VisAttributes(G4Colour(0.8,0.8,0.8));     //grey
  G4VisAttributes *inDeadTubeAttr = new G4VisAttributes(G4Colour(0.,0.4,0.3));   //tale
  G4VisAttributes *BoreholeTubeAttr = new G4VisAttributes(G4Colour(0.,0.,1.));   //blue
  G4VisAttributes *PlexiTubeAttr = new G4VisAttributes(G4Colour(0.8,0.8,1.));   //gray
//  G4VisAttributes *VerticalPbAttr = new G4VisAttributes(G4Colour(1.,1.,1.));
//  G4VisAttributes *HorizontalPbAttr = new G4VisAttributes(G4Colour(1.,1.,1.));
  G4VisAttributes *FDLWConeAttr = new G4VisAttributes(G4Colour(0.,1.,0.));    //gree
  G4VisAttributes *FrontGeConeAttr = new G4VisAttributes(G4Colour(0.,1.,0.));    //gree
/*  VerticalPbAttr->SetVisibility(true);
  VerticalPbAttr->SetForceWireframe(true);
  vertPb_log->SetVisAttributes(VerticalPbAttr);

  HorizontalPbAttr->SetVisibility(true);
  HorizontalPbAttr->SetForceWireframe(true);
  horPb_log->SetVisAttributes(HorizontalPbAttr);
*/

  PlexiTubeAttr->SetVisibility(true);
  PlexiTubeAttr->SetForceWireframe(true);
  Plexi_log->SetVisAttributes(PlexiTubeAttr);

  MgWTubeAttr->SetVisibility(true);
  MgWTubeAttr->SetForceWireframe(true);
  MgW_log->SetVisAttributes(MgWTubeAttr);
  MgW_log2->SetVisAttributes(MgWTubeAttr);

  MgTubeAttr->SetVisibility(true);
  MgTubeAttr->SetForceWireframe(true);
  Mg_log->SetVisAttributes(MgTubeAttr);
```

```
Mg_log2->SetVisAttributes(MgTubeAttr);

AlTubeAttr->SetVisibility(true);
AlTubeAttr->SetForceWireframe(true);
Al_log->SetVisAttributes(AlTubeAttr);
Al_log2->SetVisAttributes(AlTubeAttr);

AlWTubeAttr->SetVisibility(true);
AlWTubeAttr->SetForceWireframe(true);
AlW_log->SetVisAttributes(AlWTubeAttr);
AlW_log2->SetVisAttributes(AlWTubeAttr);

VacuumTubeAttr->SetVisibility(true);
VacuumTubeAttr->SetForceWireframe(true);
Vacuum_log->SetVisAttributes(VacuumTubeAttr);
Vacuum_log2->SetVisAttributes(VacuumTubeAttr);

InVacuumTubeAttr->SetVisibility(true);
InVacuumTubeAttr->SetForceWireframe(true);
InVacuum_log->SetVisAttributes(InVacuumTubeAttr);
InVacuum_log2->SetVisAttributes(InVacuumTubeAttr);

FDLWConeAttr->SetVisibility(true);
FDLWConeAttr->SetForceWireframe(true);
FDLW_log->SetVisAttributes(FDLWConeAttr);
FDLW_log2->SetVisAttributes(FDLWConeAttr);

FrontGeConeAttr->SetVisibility(true);
FrontGeConeAttr->SetForceWireframe(true);
frontGeCone_log->SetVisAttributes(FrontGeConeAttr);
frontGeCone_log2->SetVisAttributes(FrontGeConeAttr);

outDeadTubeAttr->SetVisibility(true);
outDeadTubeAttr->SetForceWireframe(true);
outDead_log->SetVisAttributes(outDeadTubeAttr);
outDead_log2->SetVisAttributes(outDeadTubeAttr);

GeTubeAttr->SetVisibility(true);
GeTubeAttr->SetForceWireframe(true);
Ge_log->SetVisAttributes(GeTubeAttr);
Ge_log2->SetVisAttributes(GeTubeAttr);

inDeadTubeAttr->SetVisibility(true);
inDeadTubeAttr->SetForceWireframe(true);
inDead_log->SetVisAttributes(inDeadTubeAttr);
inDead_log2->SetVisAttributes(inDeadTubeAttr);

BoreholeTubeAttr->SetVisibility(true);
BoreholeTubeAttr->SetForceWireframe(true);
Borehole_log->SetVisAttributes(BoreholeTubeAttr);
Borehole_log2->SetVisAttributes(BoreholeTubeAttr);
```

```
  return World_phys;
}
```

References

[1]   Keiichi Shibata, Journal of Nuclear Science and Technology, 49, 824–835, (2012)

[2]   Generation-IV International Forum, www.gen-4.org

[3]   N. Dzysiuk, A. Kadenko, I. Kadenko, and G. Primenko, Phys. Rev. C. 86, 034609 (2012)

[4]   Junhua Luo, Rong Liu, Li Jiang, Zhenlai Liu, Journal of Radioanalytical and Nuclear Chemistry
      289, 1 (2011)

[5]   Xiangzhong Kong, Yongchang Wang, Jingkang Yang, Applied Radiation and Isotopes 49, 12 (1998)

[6]   H. Liljavirta and T. Tuurnala, Physica Scripta 18, 2 (1978)

[7]   S. M. Qaim, Nuclear Physics A 224, 2 (1974)

[8]   P.Rama Prasad, J. Rama Rao, and E. Kondaiah, Nuclear Physics A 125, 1 (1969)

[9]   N. Lakshmana Das, C. V. Srinivasa Rao, B. V. Thirumala Rao, J. Rama Rao, Pramana 17, 1 (1981)

[10] E. Havlik, Acta Phys. Austr. 34, 209 (1971)

[11] T. Bari, Dissertation Abstracts B 32, 5091 (1972)

[12] Εισαγωγή στις Πυρηνικές Αντιδράσεις, G.R. Satchler,   Μετάφραση Ν Νικολής Εκδόσεις
      Πελεκάνος

[13] N. Patronis et al, Phys. Rev. C 69, 025803 (2004)

[14] Measurement and Detection Radiation, Nicholas Tsoulfanidis, Taylor & Francis (1798)

[15] C. W. Reich, Nuclear Data Sheets 112, 2497 (2011)

[16] R. B. Firestone, Nuclear Data Sheets 108, 2319 (2007)

[17] Huang Xialong, Nuclear Data Sheets 108, 1093 (2007)

[18] Coral M. Baglin, Nuclear Data Sheets 113, 2187 (2012)

[19] Evert Birgesson and Goran Lovestam, Software Manual, NeuSDesc-Neutron Sources Description,
      IRMM, 2007

[20] Yang Dong, Huo Junde, Nuclear Data Sheets 121, 1 (2014)

[21] M. J. Martin, Nuclear Data Sheets 114, 1497 (2013)

[22] International Reactor Dosimetry and Fusion File IRDFF v.1.05, 09 October, 2014

Bibliography

[1]   N. Patronis, C. T. Papadopoulos, S. Galanopoulos, M. Kokkoris, G. Perdikakis, and R.
      Vlastou,Physical Review C 75, 034607 (2007)

[2]   Undergraduate thesis, University of Ioannina (2014), Zinovia Eleme

[3]   M.Sc. Thesis, N.T.U.A. (2013), Antigoni Kalamara

[4]   M.Sc. Thesis, N.T.U.A. (2011), Andreas Tsinganis

[5]   Neutron Cross Sections, Donald J. Hughes, Pergamon Press (1957)

[6]   Radiation Detection and Measurement, Glenn F. Knoll, John Wiley & Sons (2000)